RESEARCH MEMORANDUM

FREE-FLIGHT SKIN TEMPERATURE AND PRESSURE MEASUREMENTS ON A SLIGHTLY BLUNTED 25° CONE-CYLINDER-FLARE CONFIGURATION TO A MACH NUMBER OF 9.89

By Aleck C. Bond and Charles B. Rumsey

Langley Aeronautical Laboratory
Langley Field, Va.

NATIONAL ADVISORY COMMITTEE
FOR AERONAUTICS

WASHINGTON
April 10, 1957

NATIONAL ADVISORY COMMITTEE FOR AERONAUTICS

RESEARCH MEMORANDUM

FREE-FLIGHT SKIN TEMPERATURE AND PRESSURE MEASUREMENTS ON A SLIGHTLY BLUNTED 25° CONE-CYLINDER-FLARE CONFIGURATION TO A MACH NUMBER OF 9.89

By Aleck C. Bond and Charles B. Rumsey

SUMMARY

Skin temperatures and surface pressures have been measured on a slightly blunted cone-cylinder-flare configuration to a maximum Mach number of 9.89 with a rocket-propelled model. The cone had a total angle of 25° and the flare had a 10° half-angle. Temperature data were obtained at eight cone locations, four cylinder locations, and seven flare locations; pressures were measured at one cone location, one cylinder location, and three flare locations. Four stages of propulsion were utilized and a reentry type of trajectory was employed in which the high-speed portion of flight was obtained by firing the last two stages during the descent of the model from a peak altitude of 99,400 feet. The Reynolds number at peak Mach number was 1.2×10^6 per foot of model length. The model length was 6.68 feet. During the higher speed portions of flight, temperature measurements along one element of the nose cone indicated that the boundary layer was probably laminar, whereas on the opposite side of the nose the measurements indicated transitional or turbulent flow. Temperature distributions along one meridian of the model showed the flare to have the highest temperatures and the cylinder generally to have the lowest. A maximum temperature of 970° F was measured on the cone element showing the transitional or turbulent flow; along the opposite side of the model, the maximum temperatures of the cone, cylinder, and flare were 545° F, 340° F, and 680° F, respectively, at the corresponding time.

INTRODUCTION

A program for the investigation of aerodynamic heat transfer and boundary-layer transition on bodies in free flight at supersonic and hypersonic speeds is being conducted by the Langley Pilotless Aircraft Research Division. Early results of this program have provided measurements of turbulent heat transfer at single points on 10° total-angle

conical noses at supersonic speeds (refs. 1 and 2) and more recent results have provided temperature distributions and hence aerodynamic heat transfer to parabolic bodies and 10° and 15° total-angle cones (refs. 3, 4, and 5) at still higher supersonic speeds.

The exploratory hypersonic flight test reported in reference 6 demonstrated the feasibility of the four-stage vehicle for obtaining hypersonic test speeds and provided valuable information for developing flight techniques. The present test utilized four stages of propulsion and provided more extensive instrumentation in the test model. The configuration of the test model was a slightly blunted cone-cylinder-flare configuration which was developed from the design of the model of reference 5. (The cone had a total angle of 25° and the flare had a 10° half-angle.) The purpose of the present test was to investigate the heat transfer and nature of the boundary layer over the configuration as well as the pressure distributions near and on the flare at hypersonic speeds.

The flight test was conducted at the Langley Pilotless Aircraft Research Station at Wallops Island, Va. A maximum Mach number of 9.89 was attained and telemetered data were obtained during the flight to approximately 1.5 seconds after maximum Mach number was reached. In order to expedite this presentation, no analysis of the heating data nor detailed examination of the pressure data has been included.

SYMBOLS

C_p	pressure coefficient, $\frac{p - p_o}{q}$
M	Mach number
p	pressure
q	dynamic pressure
R	Reynolds number
T	temperature
t	time
V	velocity
V_c	velocity of sound

X length from zero station

ρ density of air

Subscripts:

o undisturbed free stream ahead of model

w wall

N nose (X = 1.73)

C cylinder (X = 58.73)

1 flare (X = 61.07)

2 flare (X = 66.95)

3 flare (X = 73.11)

MODEL AND INSTRUMENTATION

Model Configuration

The model was a body of revolution 6.68 feet long with a blunted 25° cone nose section, a cylindrical midsection, and a 10° half-angle flare tail section. Figure 1 is a sketch showing pertinent details and dimensions of the model and figures 2, 3, and 4 show photographs of the model. The conical nose was spun from Inconel sheet approximately 0.032 inch thick. The blunt tip was machined from Inconel and was welded to the nose skin. Details of the nose tip are shown in the sketch of figure 1. The nose was blunted in order to eliminate melting of the sharp tip during the high-heating period of the flight. A nearly flat-faced blunting was chosen in lieu of a hemispherical tip since the larger radius of this flat type of blunting provides lower heat transfer to the nose tip. The three external channels along the cylindrical portion of the body provided cable conduits from the telemeter in the nose to the power plugs and antenna at the base of the flare. The channels were equally spaced around the cylinder and welded to it. The cylinder and the 10° half-angle flare section were both rolled from 0.032-inch-thick Inconel and welded together. The flare skin was backed by balsa wood to aid in maintaining the conical shapes.

Prior to assembly, the nose, cylinder, and flare sections were polished and then heat-treated in order to establish an oxidized skin surface whose emissivity would not change radically as the skin heated

during the flight. The oxide coating was removed from the forward $2\frac{3}{4}$ inches of the blunted nose, and this portion of the nose was highly polished as can be seen in the photograph (fig. 3). The oxide coating was also removed near the juncture of the nose cone and cylinder at assembly of these sections. Pertinent physical properties of the Inconel skin are given in figure 5 which shows curves from reference 7 of conductivity, specific heat, and the emissivity for an oxidized surface as functions of temperature.

Surface roughness of the model skin was measured with a Physicists Research Company Profilometer. The measured roughnesses, in microinches (rms), were as follows: prior to oxidizing, 3.5 to 7 on the nose cone, 10 to 20 on the cylinder, and 2 to 3 on the flare; after oxidizing, 10 to 12 on the oxidized nose surface and 2 to 3 on the highly polished forward portion of the nose. Roughness measurements were not made on the cylinder and flare after oxidizing.

Instrumentation

Twenty-four temperatures, five pressures, the thrust acceleration, and the drag deceleration were telemetered from the model during flight. The telemeter was carried in the nose section and was protected from the high nose-skin temperatures reached during the test by a radiation shield. The shield consisted of a cone rolled from 0.032-inch-thick Inconel, spaced approximately 1/4 inch inside the external nose skin and supported by the solid nose tip at the forward end and by a bulkhead at the rear of the nose section.

One pressure orifice was located near the forward end of the nose section, another on the cylinder just forward of the cylinder-flare junction, and three were located along the flare section, at the stations indicated in figure 1. All the orifices were on a longitudinal line along the skin which lay midway between two of the external channels.

Twenty-three thermocouples were installed on the skin of the model at the locations indicated in figure 1, and one was located on the radiation shield. The eleven thermocouples on the nose skin were located along two longitudinal lines 180° apart circumferentially, six along the upper line and five at nearly duplicate stations along the lower line. The upper line was located so that, with respect to the cylinder, it lay midway between two of the external channels (120° from the line of the pressure orifices). Along this upper line, five thermocouples were also located on the cylinder and seven on the flare. All thermocouples were no. 30 chromel-alumel wire, with each wire of a thermocouple individually spot-welded to the inner surface of the skin approximately 3/16 inch apart circumferentially. During the flight several thermocouples failed to

operate or gave quite erratic data. These thermocouples are so noted in the table of figure 1. The measured thicknesses of the Inconel skin at the locations where the thermocouples did operate satisfactorily are given in table I.

A check of telemetered skin temperature was made just prior to launching by determining the temperatures at one of the measurement stations by means of a thermocouple taped to the exterior surface of the skin. During flight, three standard voltages and the outputs of twelve thermocouples were commutated on each of two telemeter channels so that each temperature measurement was recorded about five times per second. The three standard voltages were chosen equivalent to the lowest temperature, the midrange temperature, and the highest temperature that the skin thermocouples were expected to reach. Commutation of those known voltages along with the voltage readings of the thermocouples provided an in-flight check calibration of the thermocouple telemetering and recording system.

Other instrumentation consisted of ground-based radar units for measuring model velocity and for obtaining the position of the model in space. Velocity data were obtained by means of CW Doppler radar through burnout of the second-stage motor ($t = 29.5$ seconds), and beyond this time model velocity was obtained by integration of telemetered longitudinal acceleration and also by differentiation of the radar flight-path data (up to firing of the fourth-stage motor). A modified SCR-584 radar tracked the model until just after firing of the fourth-stage motor and provided slant range, azimuth, and elevation angle from which altitude, horizontal range, and model flight-path angle may be calculated at a given time. A modified AN/DPN-19 radar beacon installed in the forward end of the third-stage motor was used to extend the range of the SCR-584 radar beyond its normal skin tracking range. After firing of the fourth-stage motor, the flight-path data were extended by double integration of the telemetered longitudinal-acceleration data. Atmospheric data and wind conditions were measured to an altitude of 92,800 feet by means of a radiosonde launched near the time of flight and tracked by Rawin set AN/GMD-1A. Since the measured atmospheric data agreed very well with standard atmospheric conditions at the higher altitudes, standard conditions were used to extend the data through the peak altitude of the flight.

PROPULSION AND TEST TECHNIQUE

The model and boosters are shown on the launcher in figure 4. The propulsion system consisted of four stages of solid-propellant rocket motors. The first and second stages were an M6 Jato rocket motor and M5 Jato rocket motor, respectively. The third stage was a bundle of

three ABL Deacon rocket motors, which burned simultaneously, and the fourth stage was a T-40 Thiokol rocket motor. The three Deacon motors comprising the third stage were enclosed within a cylindrical skin rolled from 1/8-inch magnesium sheet, and the T-40 Thiokol fourth-stage motor was carried within the cylindrical section of the model. Locking devices between the second and third stages and between the third stage and model prevented premature separation of these stages.

The times at which the various stages were programed to fire were chosen so as to obtain the maximum Mach number without exceeding allowable skin temperatures and range restrictions. The model was launched at an elevation angle of 70° and the first two stages were used to boost the model and third-stage rocket motor to high altitude. A peak altitude of 99,400 feet was attained during coasting of the latter two stages, and the third stage was fired during the reentry of the model into the denser atmosphere at a flight-path angle of about -4° to the horizontal. About 0.7 second after burnout of the third-stage motor, the fourth stage fired and blasted the model free from the third stage. The fourth-stage motor accelerated the model to the maximum Mach number of 9.89 at an altitude of 89,600 feet. A portion of the reentry type of trajectory that the model followed as well as notations of the various stage firing times are shown in figure 6. The telemeter signal which had become progressively weaker from a time several seconds prior to third-stage firing ended completely 1.5 seconds after maximum Mach number was reached. However, almost complete time histories of the data were obtained up to this time.

FLIGHT TEST

The variation of velocity and altitude for the model through peak velocity is presented in figure 7. The mode of determination of each of these quantities, as discussed in the section entitled "Instrumentation," is also indicated. Time histories of the free-stream velocity of sound, static pressure, temperature, and density as determined from the radiosonde measurements for the model flight are presented in figure 8. The variation of flight Mach number and Reynolds number per foot with time were obtained from the data of figures 7 and 8 and are presented in figures 9 and 10, respectively.

Skin Temperatures

Representative curves of the skin temperatures measured on the nose cone, cylinder, and flare during the flight are shown in figure 11 to indicate general trends and magnitudes that occurred. The periods of skin cooling after about 10 seconds and 40 seconds correspond to the long

intervals of coasting flight after first-stage burnout and second-stage burnout, respectively. The measured temperature data for each station during the periods of strong aerodynamic heating between 24 and 42 seconds and between 92 seconds and the end of the test are shown in figures 12 and 13, respectively. (In order to facilitate presentation of the data, staggered scales have been used in many of the figures.) The temperatures measured during the first interval on the upper- and lower-nose-cone stations are shown in figures 12(a) and 12(b), respectively. The upper-nose-cone measurements indicate moderate rates of heating at the three forward stations, whereas the temperature rose much more rapidly at the most rearward station (station 14.18). The boundary layer was apparently laminar as far back as station 9.67 and transitional or turbulent at station 14.18. Examination of the measurements along the lower thermocouples (fig. 12(b)) shows temperatures and heating rates quite similar to those measured at the most rearward upper station, thus indicating a more forward transition on the lower side of the cone. A likely cause of the asymmetrical boundary layer on the nose cone may have been the nearer proximity of the nose-cone pressure orifice to the lower thermocouple line.

The temperatures measured along the cylinder from 24 to 42 seconds are shown in figure 12(c). The heating of the cylinder was moderate in comparison with the cone heating, and the data in general show progressively higher heating in moving toward the rear of the cylinder. Figures 12(d) and 12(e) show the measured flare temperatures for the time interval between 24 and 42 seconds. The temperatures and heating rates were very similar at all the flare stations. The temperatures on the flare eventually reached higher values during this interval than did the hottest of the nose-cone stations, but the peak rate of heating on the flare was less than that on the nose cone.

Time histories of the measured temperatures for the time interval between 92 seconds and the end of the test are shown in figure 13. As previously noted, the telemeter signal had begun to get progressively weaker several seconds prior to third-stage firing. For this reason, there is somewhat more scatter in the temperature data than at the earlier times, and for several short intervals no temperature values could be obtained. The upper- and lower-nose-cone temperatures are plotted in figures 13(a) and 13(b), respectively. These data clearly show a much lower rate of heat transfer along the upper thermocouple line than along the lower line and indicate that the boundary layer was probably laminar at all measurement stations on the upper line and transitional or turbulent along the lower line. Figures 13(c) and 13(d) show the temperatures measured along the cylinder and flare, respectively. At the cylinder stations, the temperatures were similar and the heating rates were low. On the flare, the heating rates generally increased slightly with distance from the cylinder-flare juncture. Reduction of the data to local Stanton number will be necessary to determine whether the flare heating was of the laminar or turbulent level.

In spite of the fact that the thermocouples along the lower line of the nose cone did not function as long as some of the other thermocouples, the maximum measured temperature on the model was obtained at station 13.94 on the lower thermocouple line at a time of 104.6 seconds. This maximum temperature was 970° F, whereas, along the opposite side of the model, the maximum temperatures of the cone, cylinder, and flare were 545° F, 340° F, and 680° F, respectively, at the corresponding time.

In figure 14, temperature distributions for the times when the flight Mach number was 6.0, 9.2, and 9.89 are presented from the data of figure 13 in order to show the relative heating over the model length. The temperatures along the cylinder were generally the lowest in all cases and the flare temperatures were of higher magnitude than any of the measurements made along the upper thermocouple line. The higher heating experienced along the lower nose thermocouple line (indicated by the shaded test points) is very clearly illustrated by this plot. Measurements at the lower cone stations were obtained at three stations only at a time of 103.5 seconds (M = 9.2) and indicate a maximum temperature of 955° F at the most rearward station as compared with the maximum upper-nose-cone temperature of 474° F and maximum flare temperature of 585° F at that time.

Pressure Coefficients

The measured pressures on the nose, cylinder, and flare were reduced to pressure coefficients and the data are presented as a function of Mach number in figures 15 and 16. In figure 15 the data for the lower speed range (up to M = 4.67) were obtained during five separate speed intervals resulting from the alternate firing and coasting of the various booster stages. These intervals are indicated by different test points in the figure. The data for all these various intervals, in general, show reasonably good agreement. The data representing the interval of coasting of the last two stages and then the subsequent firing of the third stage show more disagreement with the trends established by the prior intervals. These data are of less accuracy than those of the prior intervals since, owing to the high altitudes, the measured pressure values are in the lower part of the full-scale range of the pressure instrumentation. The erratic nature of data obtained mostly at the early part of the firing of the third stage is believed to have been caused by angle-of-attack effects, due possibly to some slight asymmetric thrust resulting from the triple rocket arrangement of the third stage.

The pressure-coefficient data for the higher speed portion of the flight were obtained during the firing of the sustainer motor in the model and are shown in figure 16. These data definitely show that the model was disturbed from its flight path as it blasted away from the third stage booster, and this disturbance caused the model to oscillate

during part of its powered flight. A mean line fairing of the pressure oscillations will produce a smooth curve which should represent near-zero-lift pressure coefficients for the various measurement locations.

In figures 15(a) and 16(a) the measured nose pressure coefficients are compared with the theoretical sharp cone pressure coefficients of reference 8. In general, the measured data are somewhat lower than the theory in the lower speed range and of slightly higher magnitude in the higher speed range. This behavior of the measured nose pressure coefficients indicates that the pressure orifice was in the region of expansion following the rapid compression caused by the blunted nose. The pressure-distribution data of reference 9, which are for a spherically tipped cone, show that the overexpansion to values below the conical values diminishes as the Mach number is increased to 3.1. The present data indicate the same trend, and, in the speed range from $M = 2.8$ to 3.4, the measured data agree quite well with cone theory. The configuration of reference 10 is more similar to the nose configuration employed on the test vehicle; however, pressure data reported in this reference are only for a Mach number of 6.85. The pressure-distribution data of reference 10 show that higher than theoretical cone pressures were obtained on a blunted 20° cone at distances up to 2 bluntness diameters back from the nose tip. In view of these data and since the nose-pressure orifice was located at less than 1 bluntness diameter from the nose tip, it is evident that the nose-cone pressure orifice was in the high-pressure expansion region during the higher speed portion of flight.

In figure 17 the nose-pressure data for the portion of flight beginning with the ignition of the third stage through the burnout of the motor in the model are replotted as a function of time. The Mach number range covered during this time is also replotted in this figure. The portion from 94 seconds to 97.8 represents flight with the third stage and the erratic nature of the nose pressure coefficient in this stage suggests the possibility of asymmetric thrust which was mentioned previously. Firing of the motor in the model at 97.8 seconds produced a disturbance that resulted in a uniform oscillation which damped in about 3 seconds, thus indicating that the dynamic stability of the model was adequate in its flight at the average altitude of 96,000 feet.

CONCLUDING REMARKS

A slightly blunted cone-cylinder-flare configuration has been flight tested by means of the rocket-model technique to a maximum Mach number of 9.89. The cone had a total angle of 25° and the flare had a 10° half-angle. A reentry type of trajectory was employed in which the high-speed portion of flight was obtained during the descent of the model from a peak altitude of 99,400 feet. A relatively large quantity of telemetered

information was obtained on the configuration, including nineteen skin temperatures and five pressures, until 1.5 seconds after maximum Mach number.

During the higher speed portion of flight, temperature measurements along one element of the nose cone indicated that the boundary layer was probably laminar, whereas on the opposite side of the nose the measurements indicated transitional or turbulent flow. Temperature distributions along one meridian of the model showed the flare to have the highest temperatures and the cylinder generally to have the lowest. On the flare, the heating rates generally increased with distance from the flare-cylinder juncture.

Langley Aeronautical Laboratory,
National Advisory Committee for Aeronautics,
Langley Field, Va., January 31, 1957.

REFERENCES

1. Rumsey, Charles B., Piland, Robert O., and Hopko, Russell N.: Aerodynamic-Heating Data Obtained From Free-Flight Tests Between Mach Numbers of 1 and 5. NACA RM L55A14a, 1955.

2. Rumsey, Charles B.: Free-Flight Measurements of Aerodynamic Heat Transfer to Mach Number 3.9 and of Drag to Mach Number 6.9 of a Fin-Stabilized Cone-Cylinder Configuration. NACA RM L55G28a, 1955.

3. Piland, Robert O., Collie, Katherine A., and Stoney, William E.: Turbulent and Laminar Heat-Transfer Measurements on a 1/6-Scale NACA RM-10 Missile in Free Flight to a Mach Number of 4.2 and to a Wall Temperature of 1400° R. NACA RM L56C05, 1956.

4. Rumsey, Charles B., and Lee, Dorothy B.: Measurements of Aerodynamic Heat Transfer and Boundary-Layer Transition on a 10° Cone in Free Flight at Supersonic Mach Numbers up to 5.9. NACA RM L56B07, 1956.

5. Rumsey, Charles B., and Lee, Dorothy B.: Measurements of Aerodynamic Heat Transfer and Boundary-Layer Transition on a 15° Cone in Free Flight at Supersonic Mach Numbers up to 5.2. NACA RM L56F26, 1956.

6. Piland, Robert O.: Performance Measurements From a Rocket-Powered Exploratory Research Missile Flown to a Mach Number of 10.4. NACA RM L54L29a, 1954.

7. O'Sullivan, William J., Jr.: Some Thermal and Mechanical Properties of Inconel at High Temperatures for Use in Aerodynamic Heating Research. Proc. A.S.T.M., vol. 55, 1955, pp. 757-763.

8. Ames Research Staff: Equations, Tables, and Charts for Compressible Flow. NACA Rep. 1135, 1953. (Supersedes NACA TN 1428.)

9. Perkins, Edward W., and Jorgensen, Leland H.: Investigation of the Drag of Various Axially Symmetric Nose Shapes of Fineness Ratio 3 for Mach Numbers From 1.24 to 3.67. NACA RM A52H28, 1952.

10. Bertram, Mitchel H.: Tip-Bluntness Effects on Cone Pressures at M = 6.85. Jour. Aero. Sci. (Readers' Forum), vol. 23, no. 9, Sept. 1956, pp. 898-900.

TABLE I

SKIN THICKNESS AT THERMOCOUPLE STATIONS

Nose

Upper line		Lower line	
Station	Thickness, in.	Station	Thickness, in.
5.64	0.0349	7.53	0.0318
7.59	.0323	9.54	.0322
9.67	.0307	11.50	.0329
14.18	.0315	13.94	.0321

Cylinder

Station	Thickness, in.
23.37	0.0321
34.37	.0315
45.37	.0323
58.57	.0337

Flare

Station	Thickness, in.
61.09	0.0327
62.77	.0328
64.44	.0329
66.41	.0330
69.37	.0329
73.70	.0324
78.72	.0317

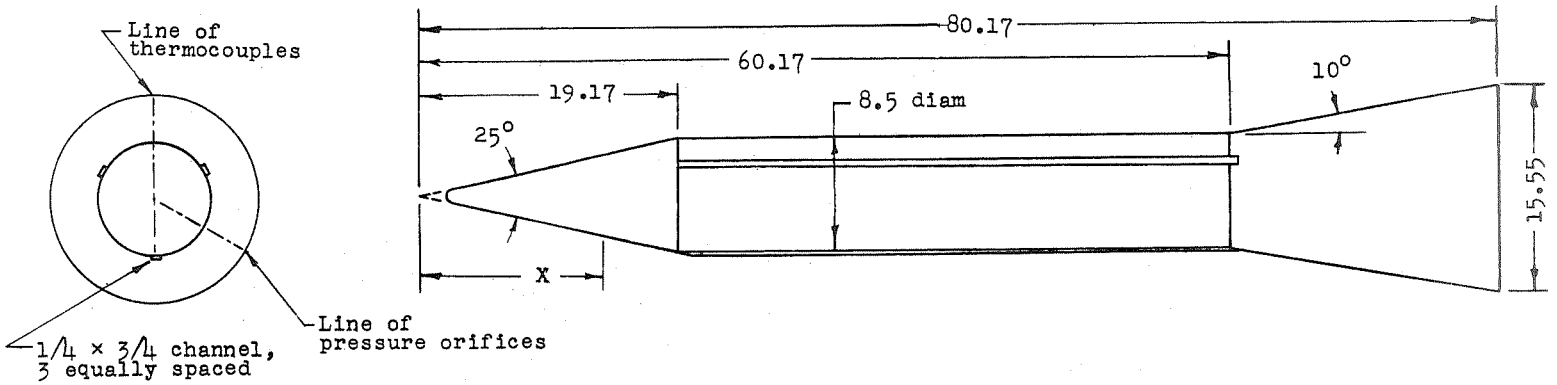

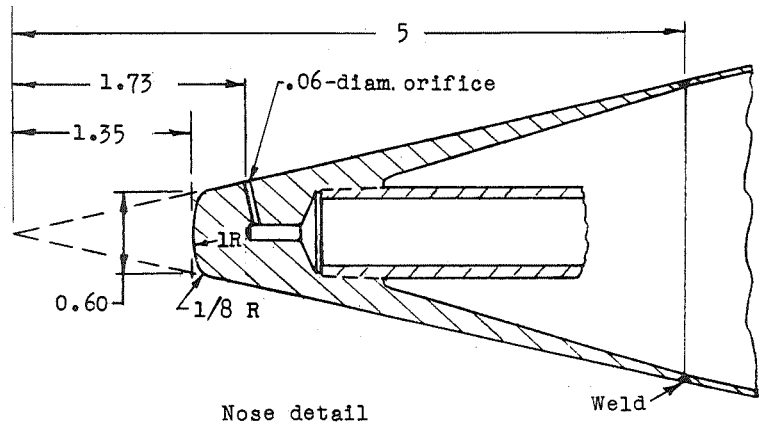

Nose detail

X for thermocouples

On nose		On Cylinder (Upper line)	On Flare (Upper line)
Upper line	Lower line		
5.64		23.37	61.09
7.59	7.53	34.37	62.77
9.67	9.54	45.37	64.44
11.62*	11.50	57.67*	66.41
14.18	13.94	58.57	69.37
17.05*	16.87*		73.70
			78.72

*did not operate

X for pressure orifices

On nose	On cylinder	On flare
1.73	58.73	61.07
		66.95
		73.11

Figure 1.- Sketch of model and detail of nose construction. All dimensions are in inches.

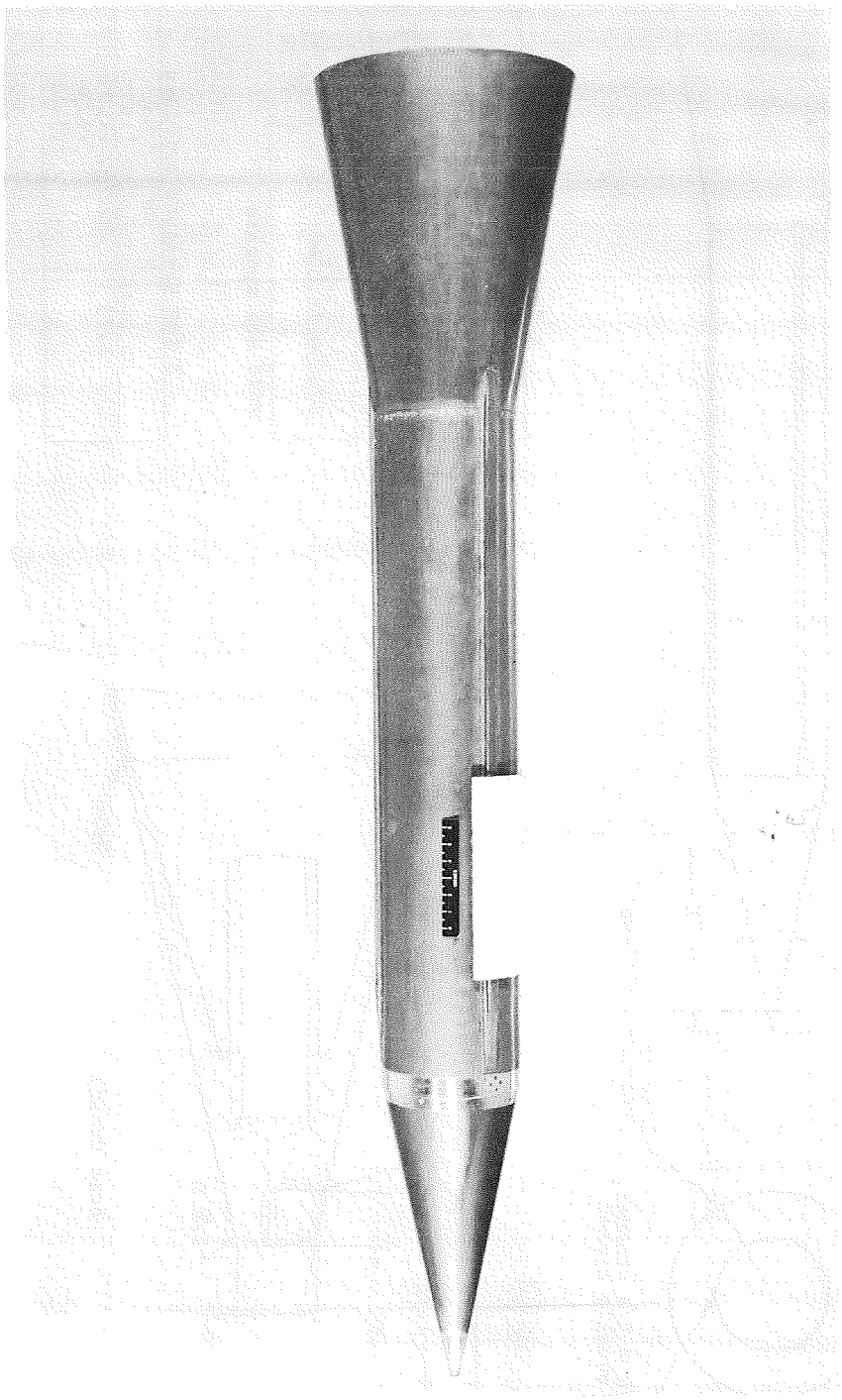

Figure 2.- Photograph of model. L-94556.1

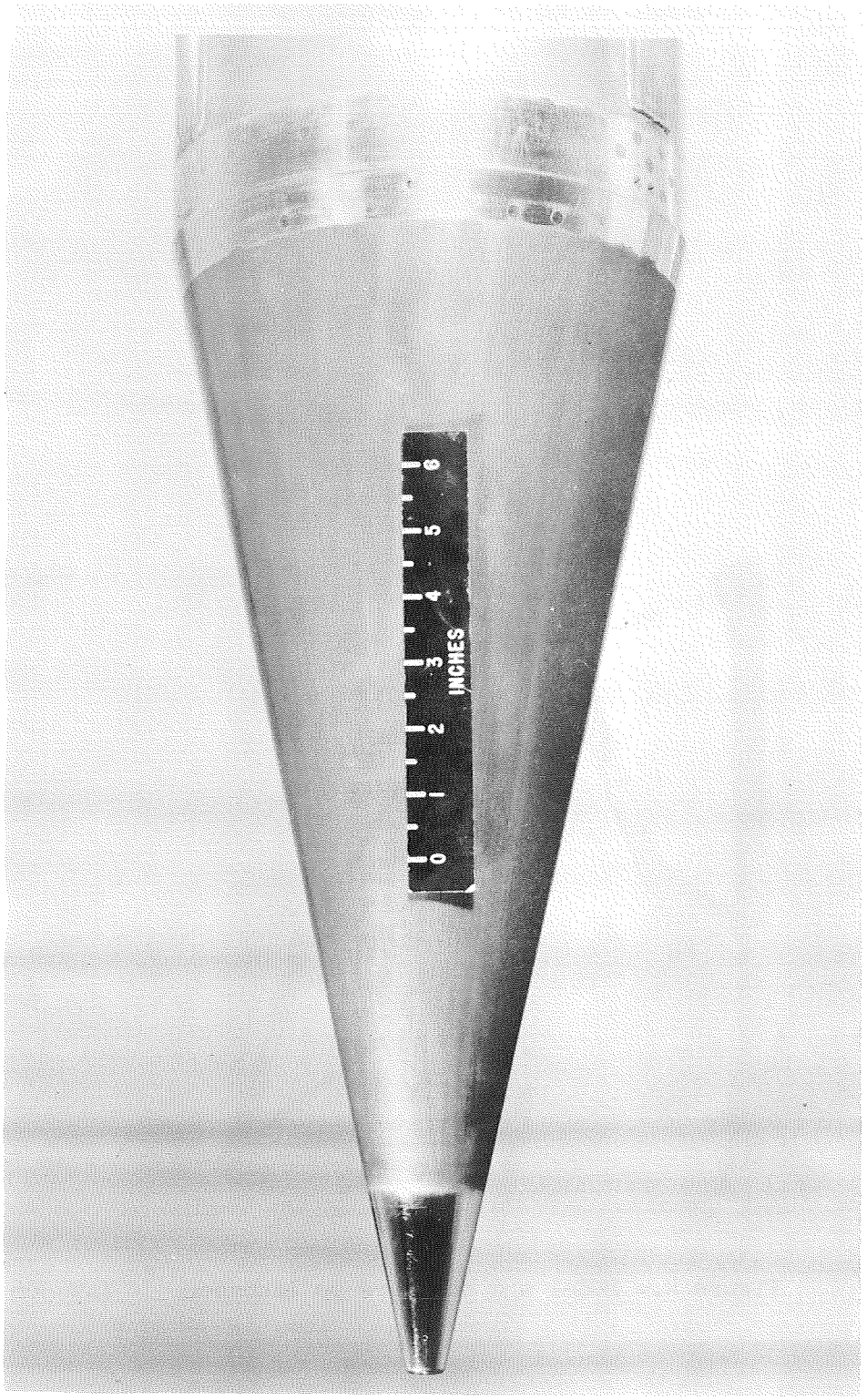

Figure 3.- Closeup photograph of model nose. L-94555

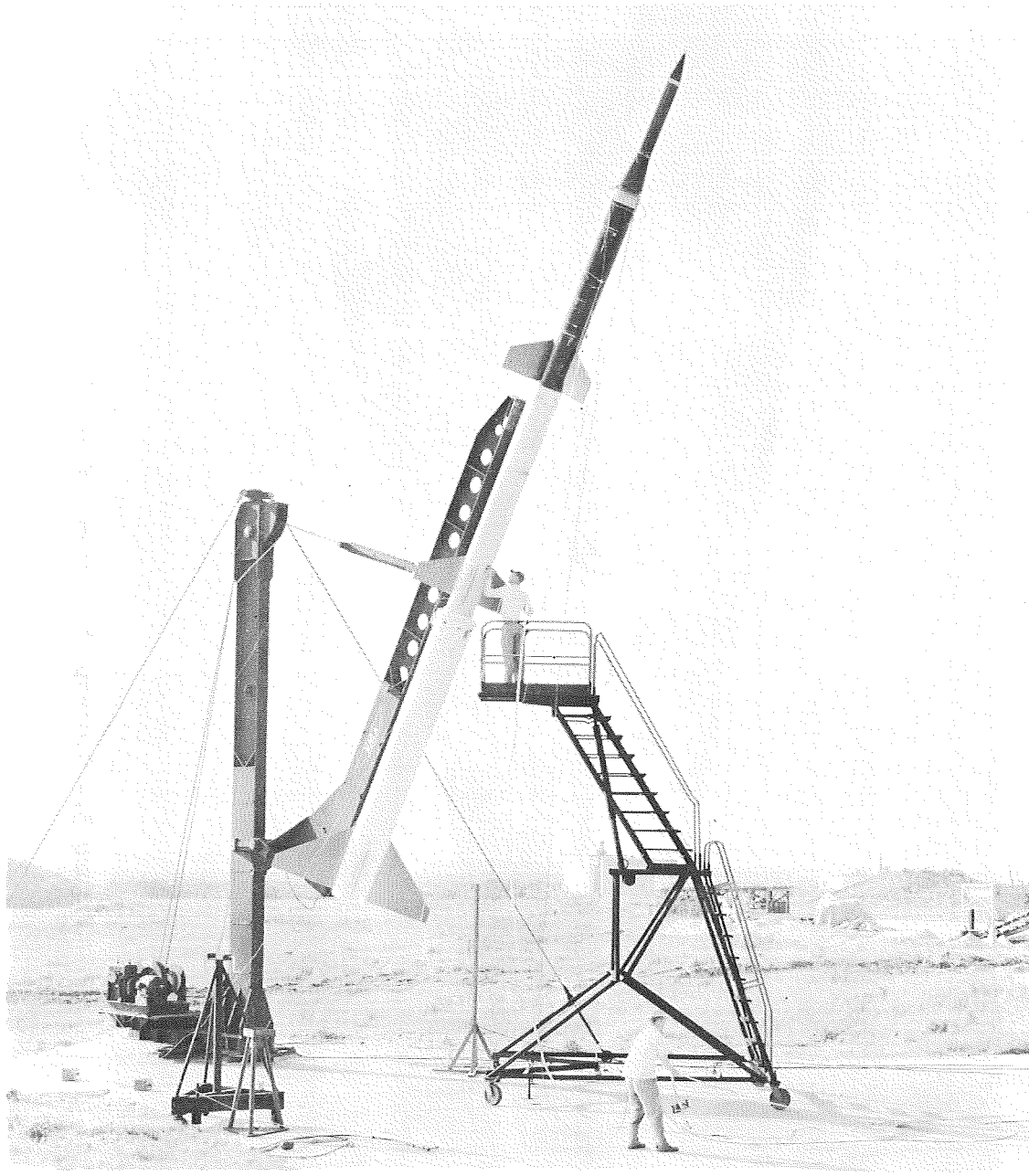

Figure 4.- Model and boosters on launcher. L-94566

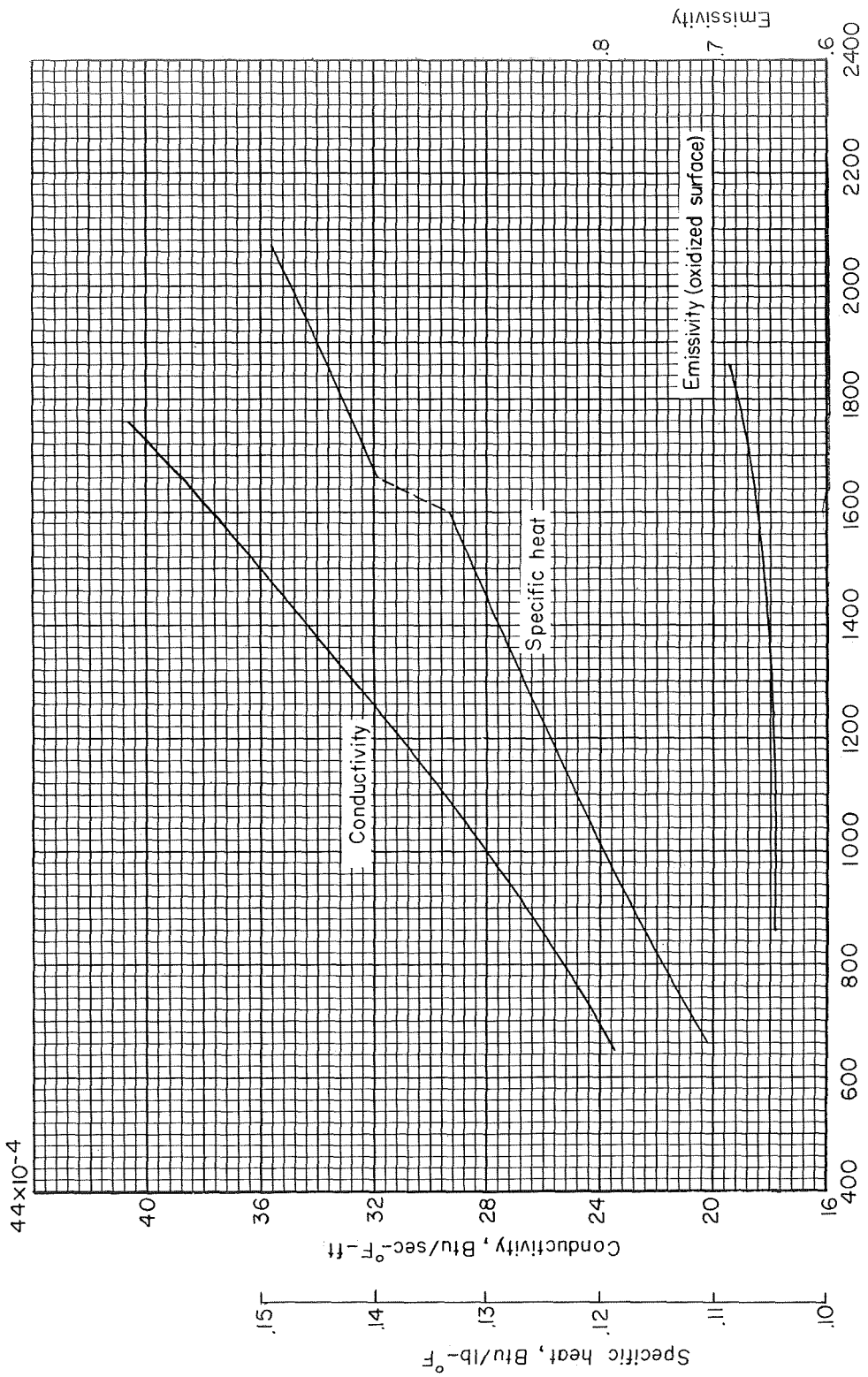

Figure 5.- Properties of annealed Inconel having 0.07-percent carbon content.

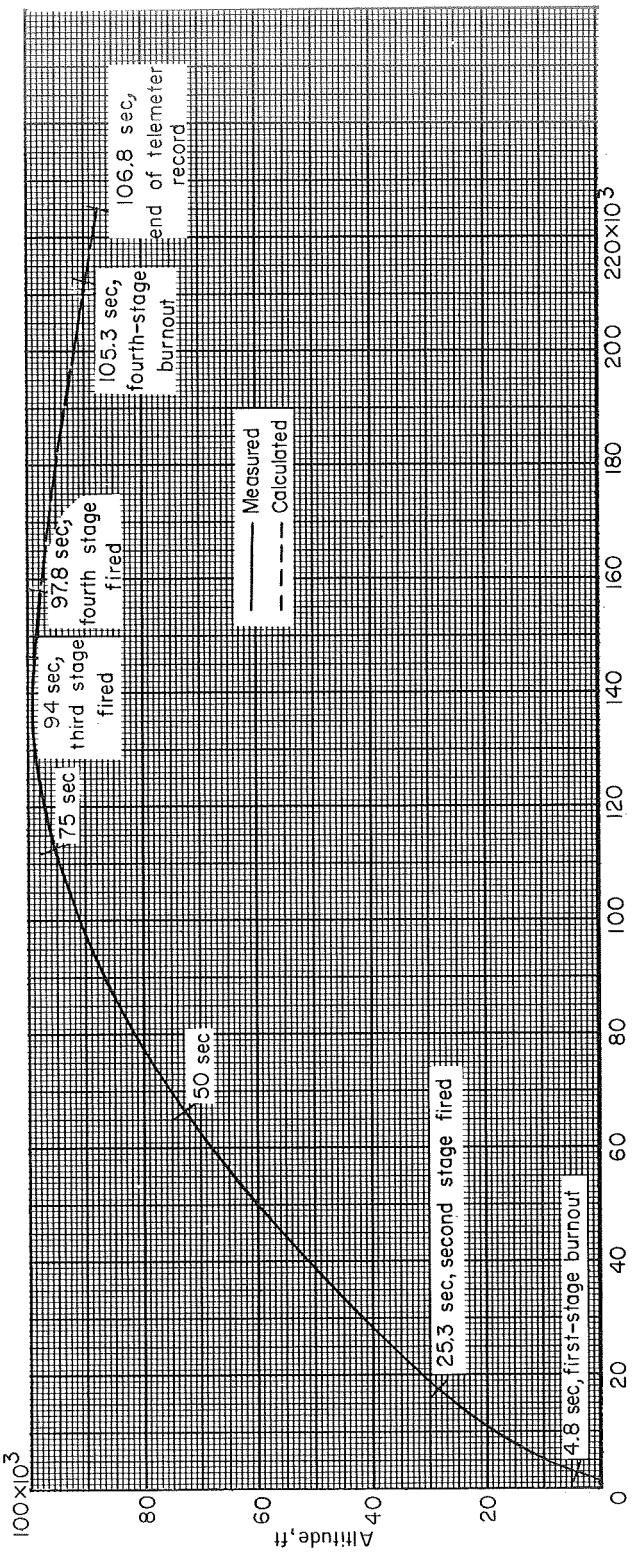

Figure 6.- A portion of the model trajectory.

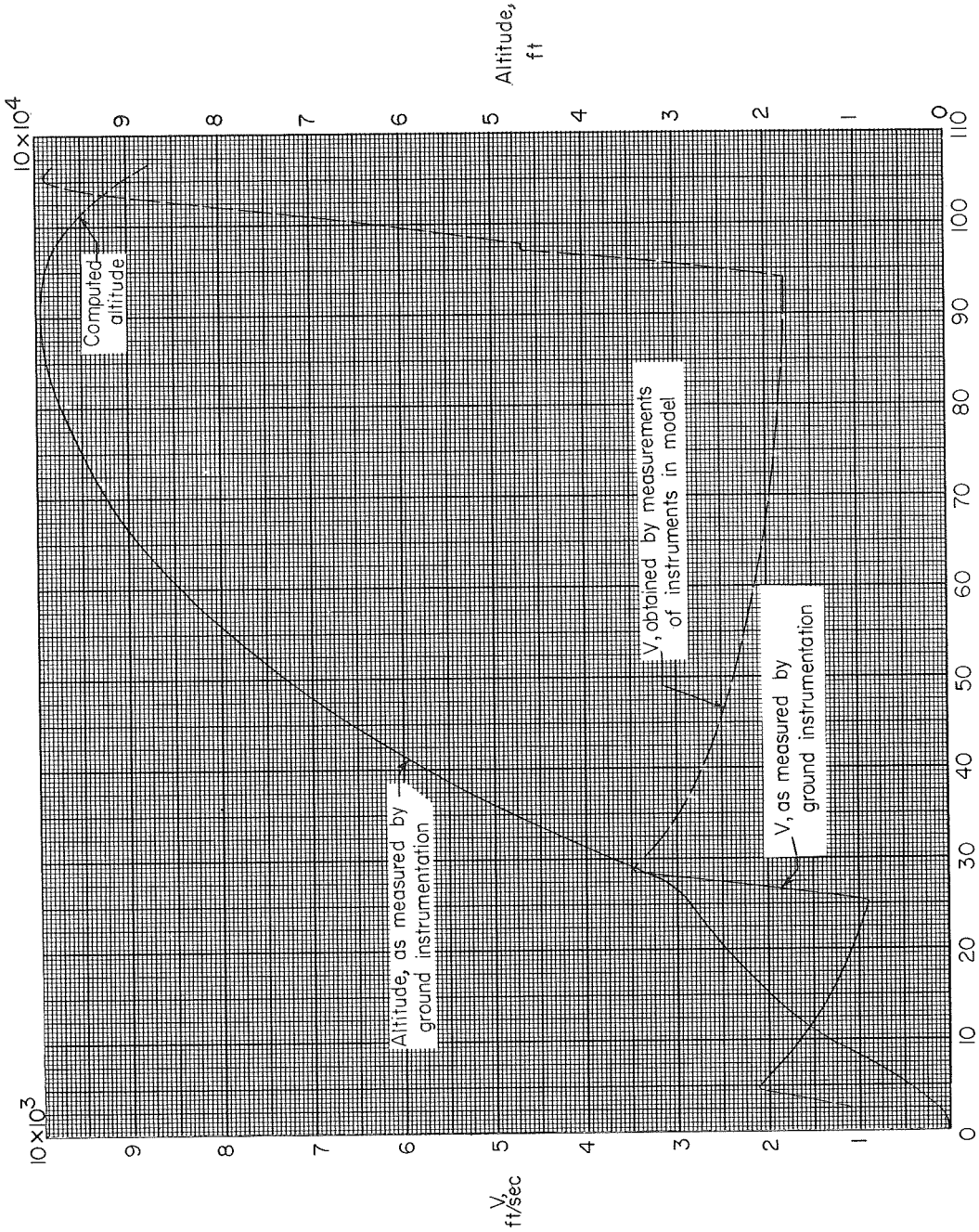

Figure 7.- Variation of altitude and velocity with time for the test vehicle.

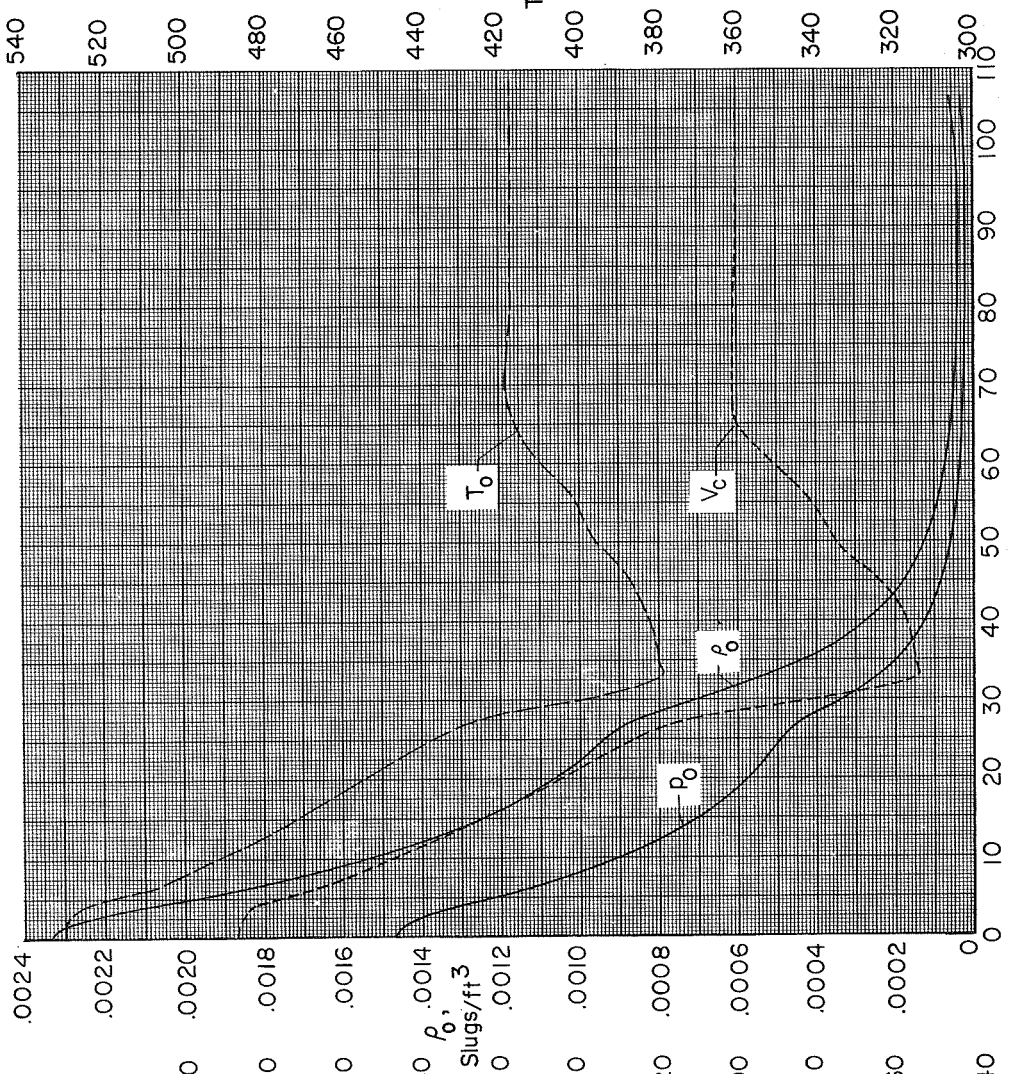

Figure 8.- Time histories of the velocity of sound, density of air, temperature, and static air pressure.

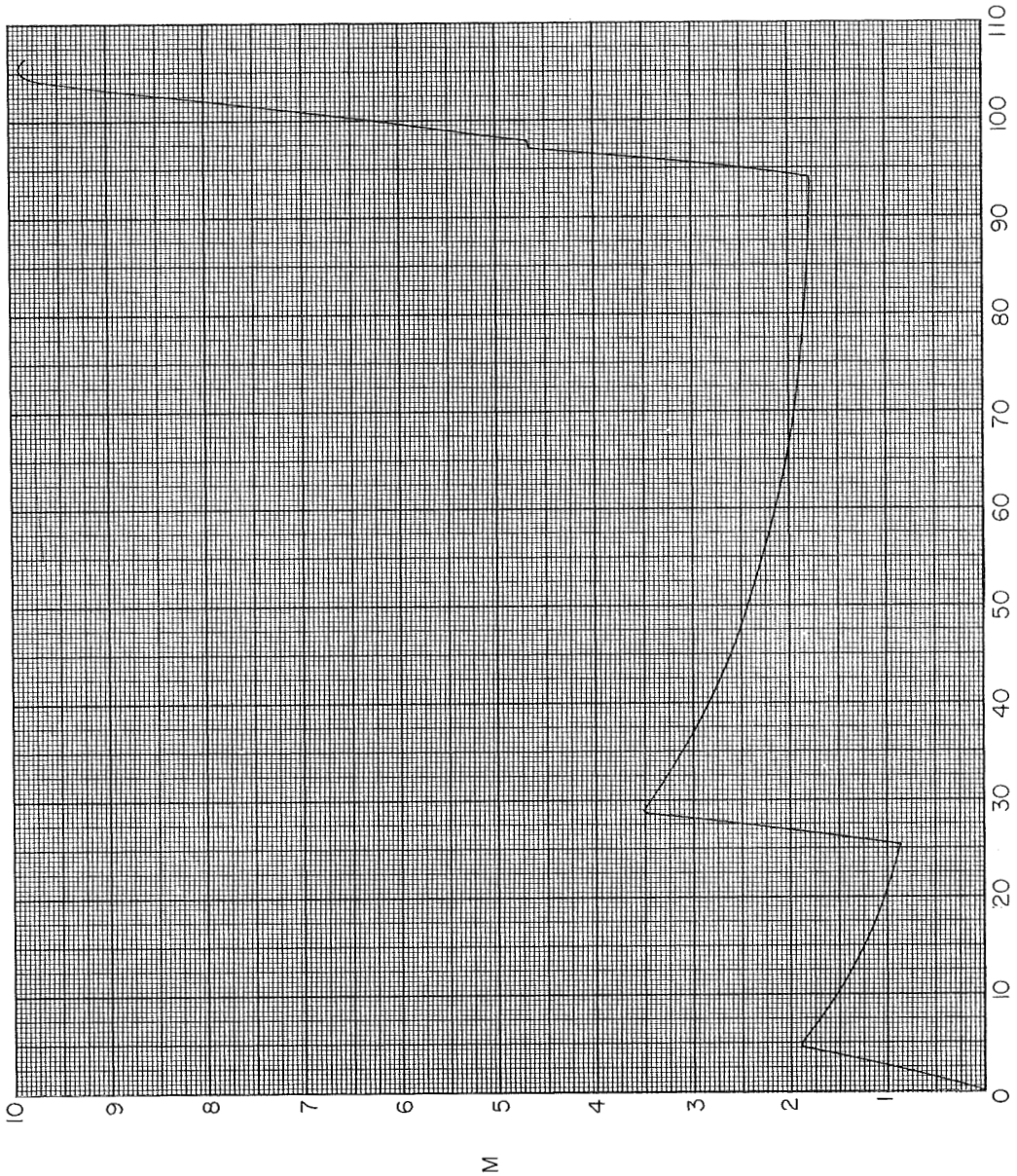

Figure 9.- Variation of Mach number with time for the test vehicle.

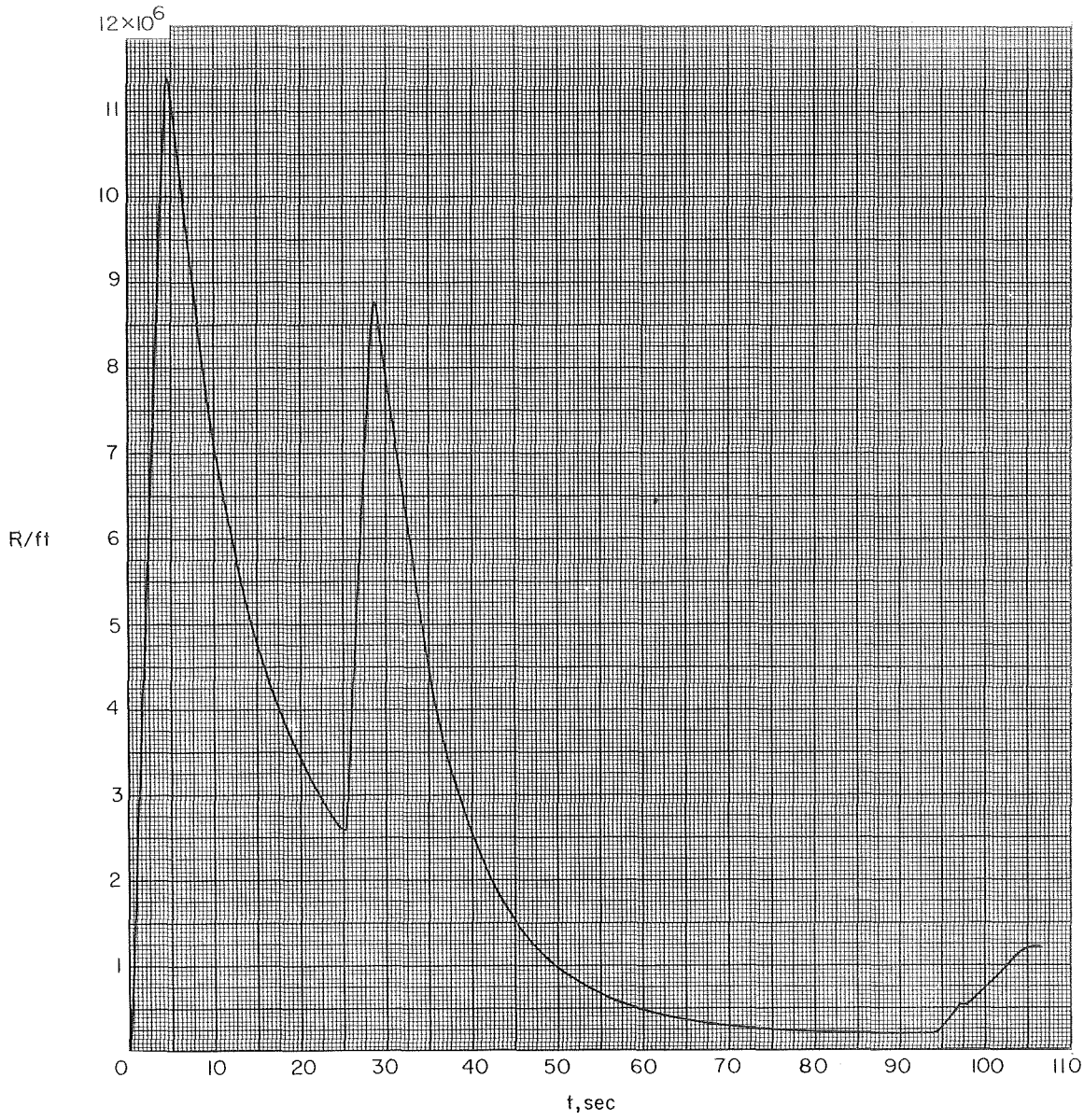

Figure 10.- Variation of Reynolds number per foot with time for the test vehicle.

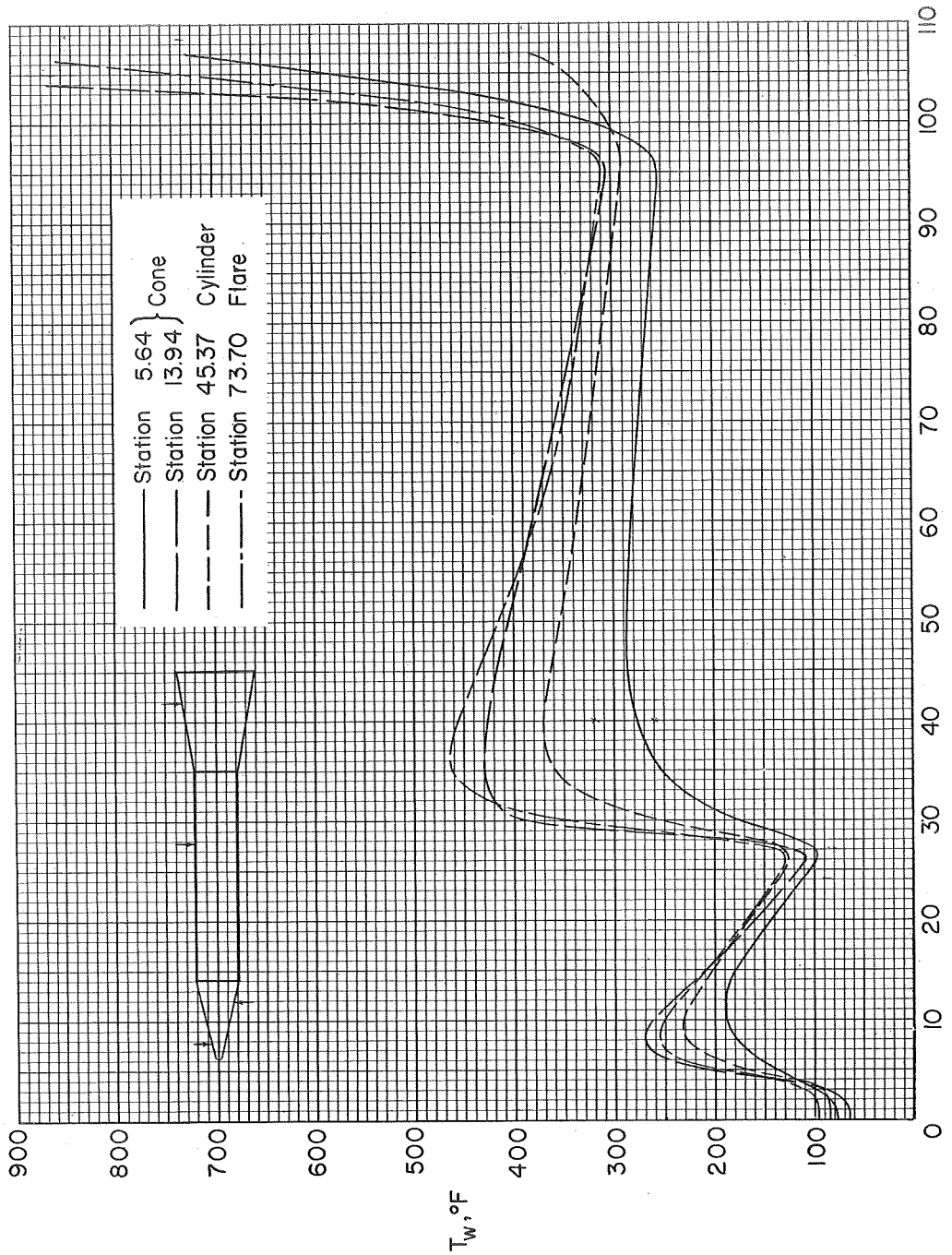

Figure 11.- Typical skin-temperature time histories as obtained from faired measurements.

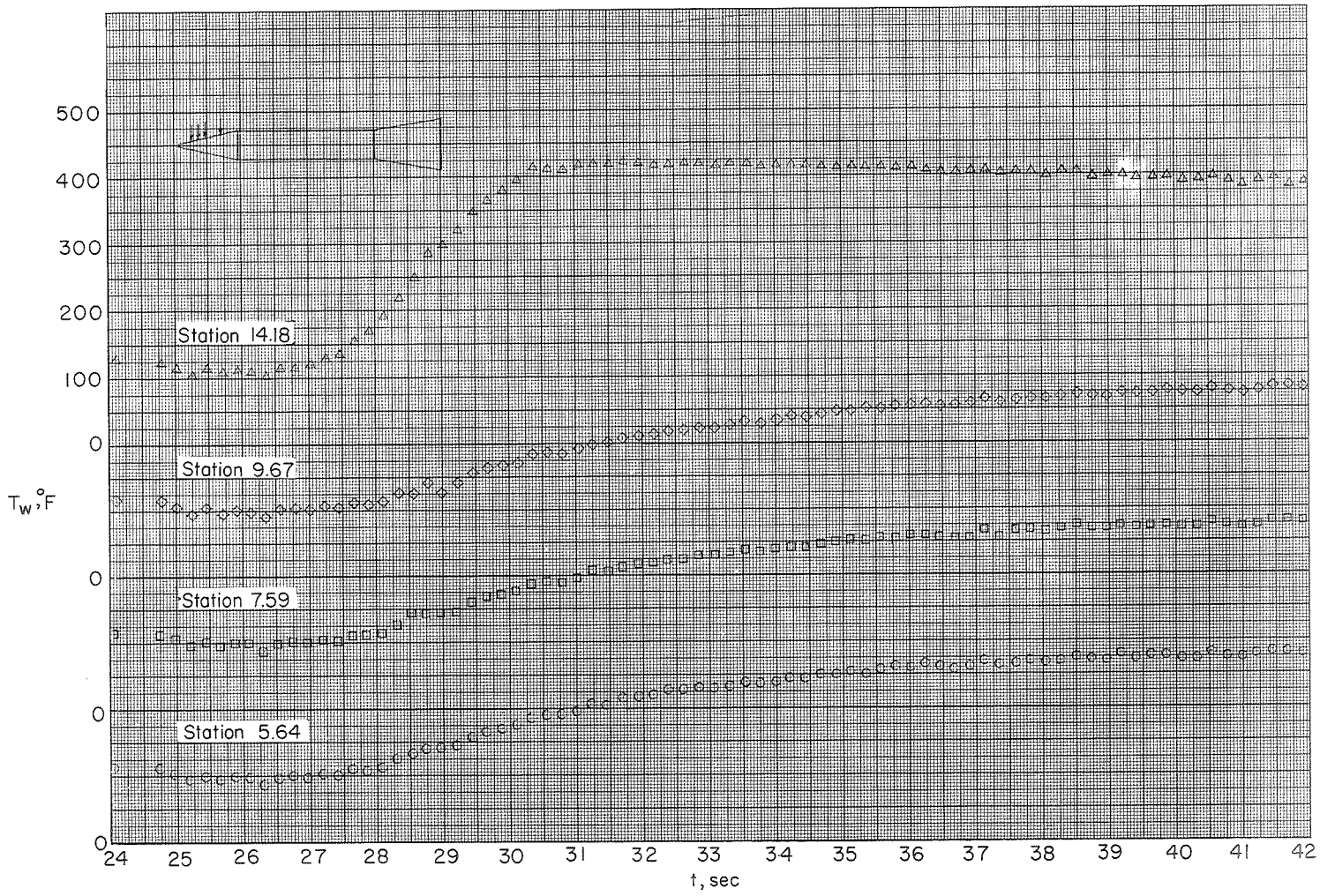

(a) Nose cone stations along upper thermocouple line.

Figure 12.- Time histories of skin temperatures over the period including the second-stage firing.

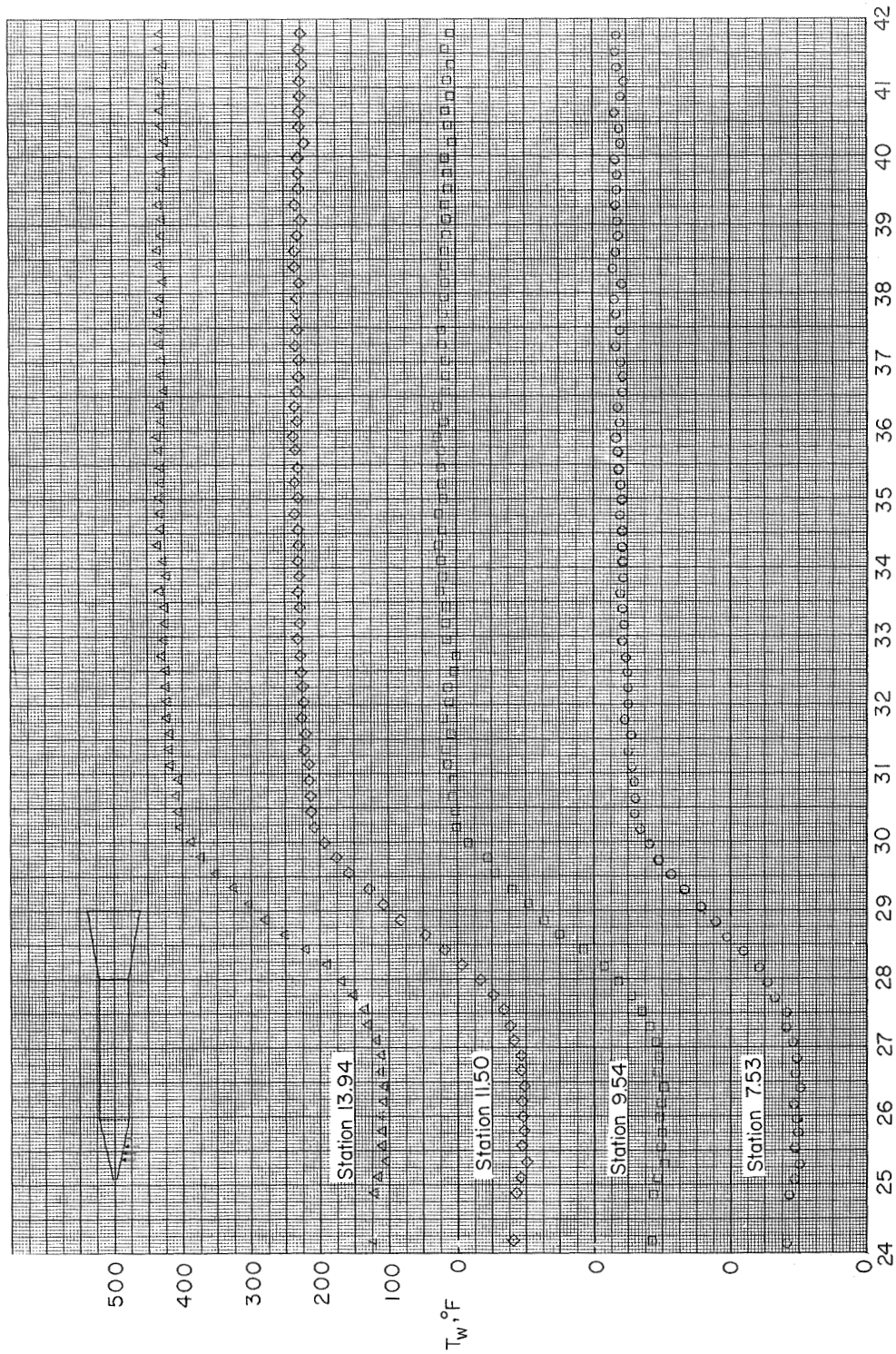

(b) Nose cone stations along lower thermocouple line.

Figure 12.- Continued.

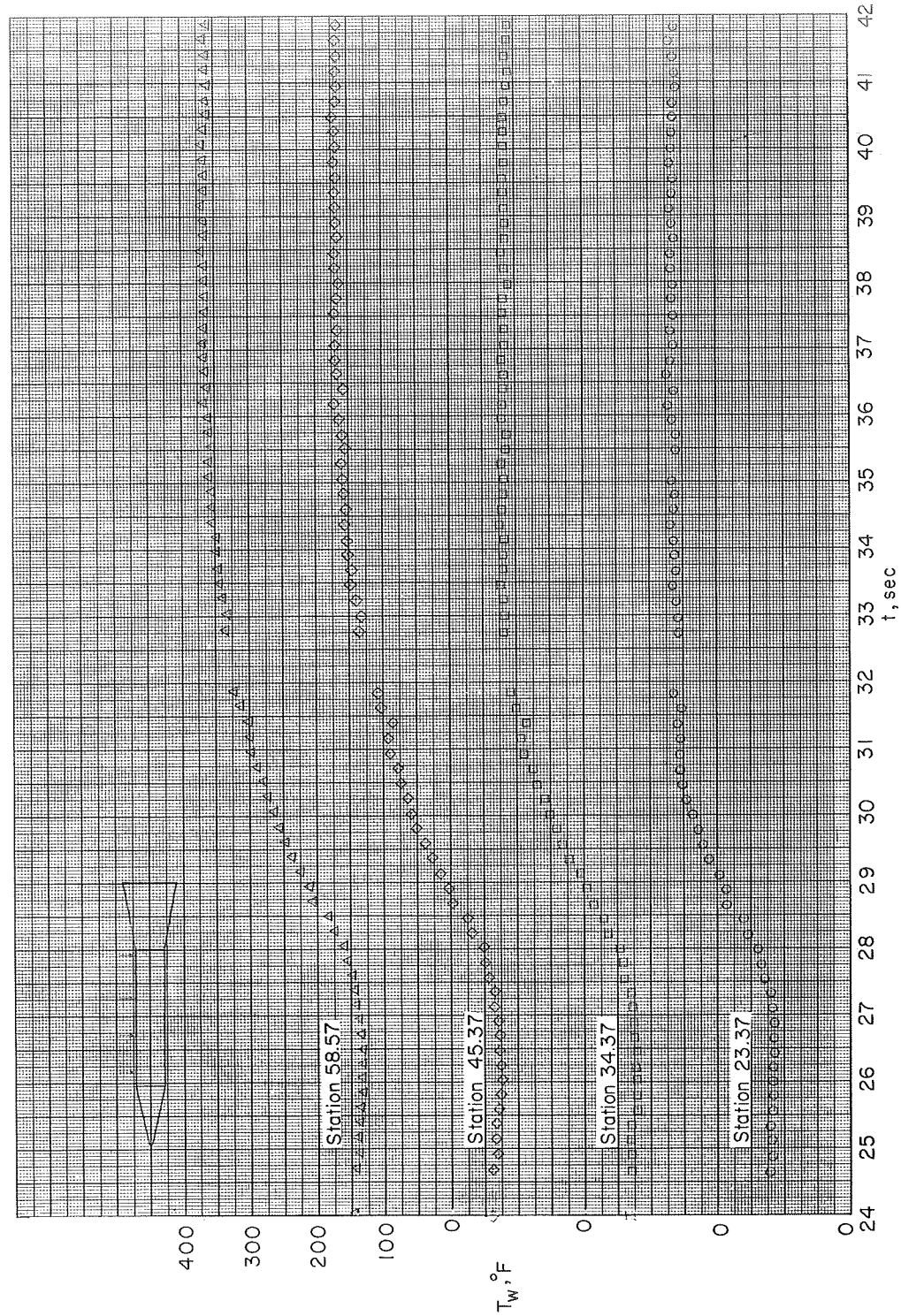

(c) Cylinder stations.

Figure 12.- Continued.

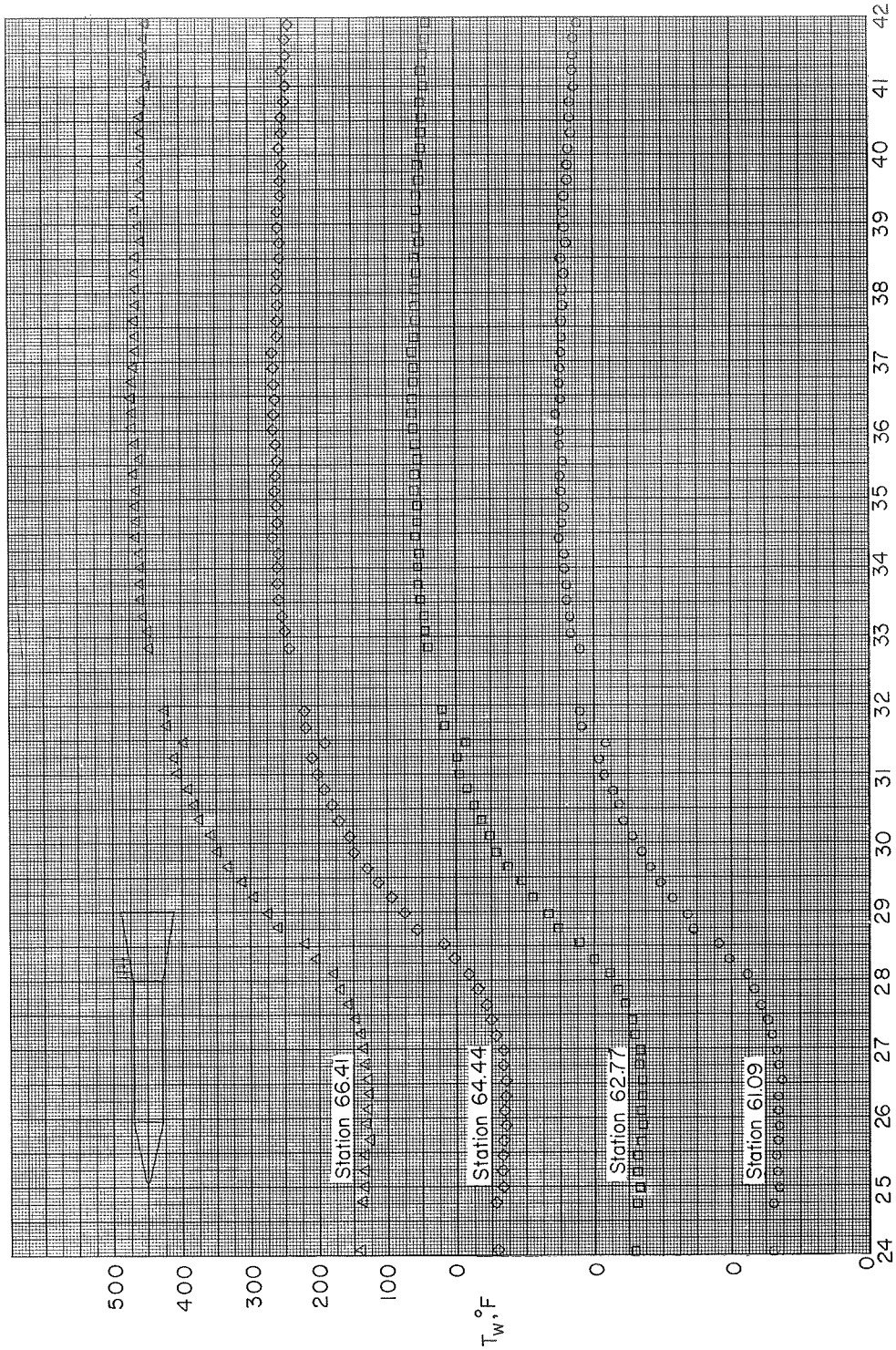

(d) Stations on forward part of flare.

Figure 12.- Continued.

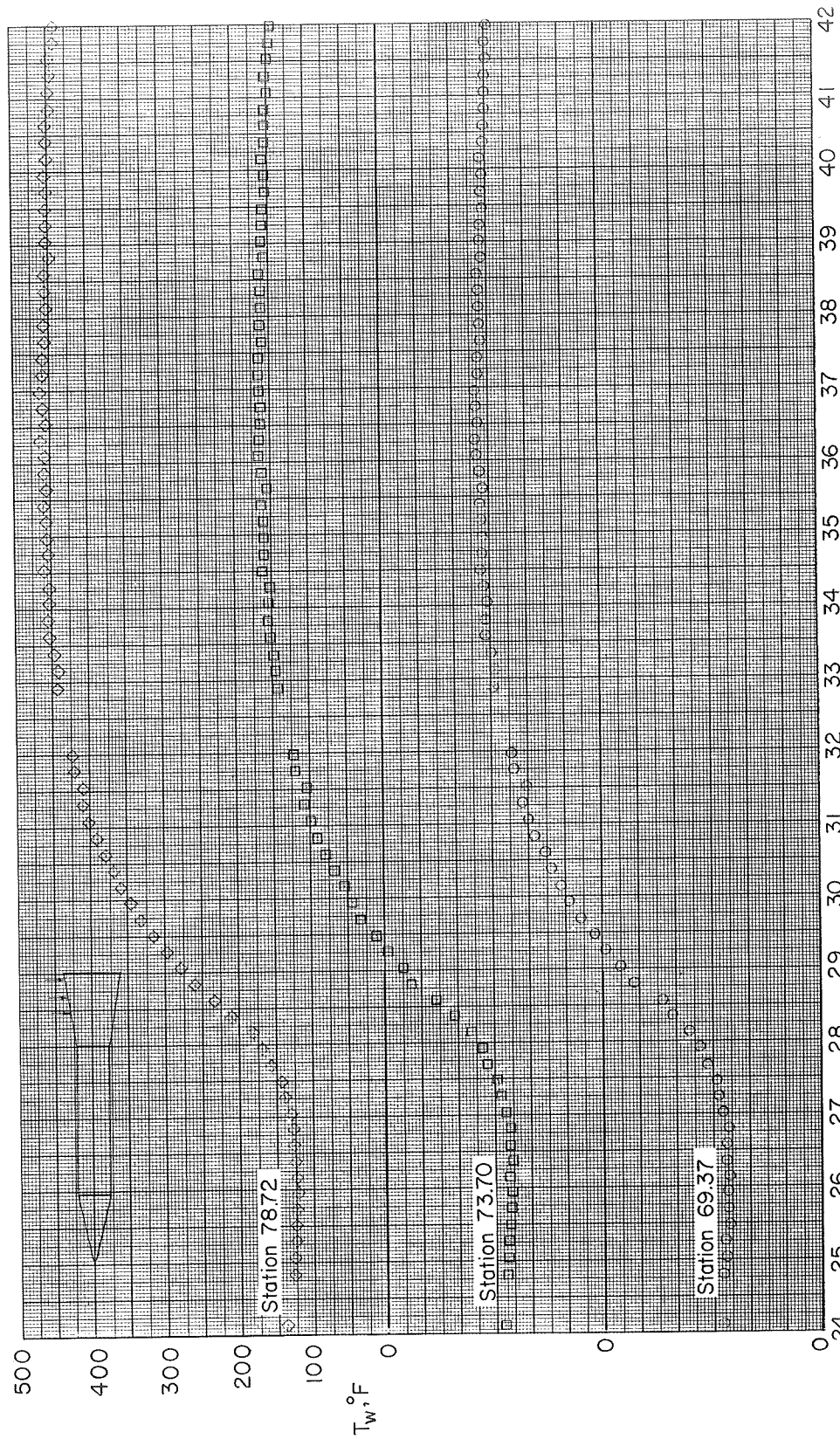

(e) Stations on rearward part of flare.

Figure 12.- Concluded.

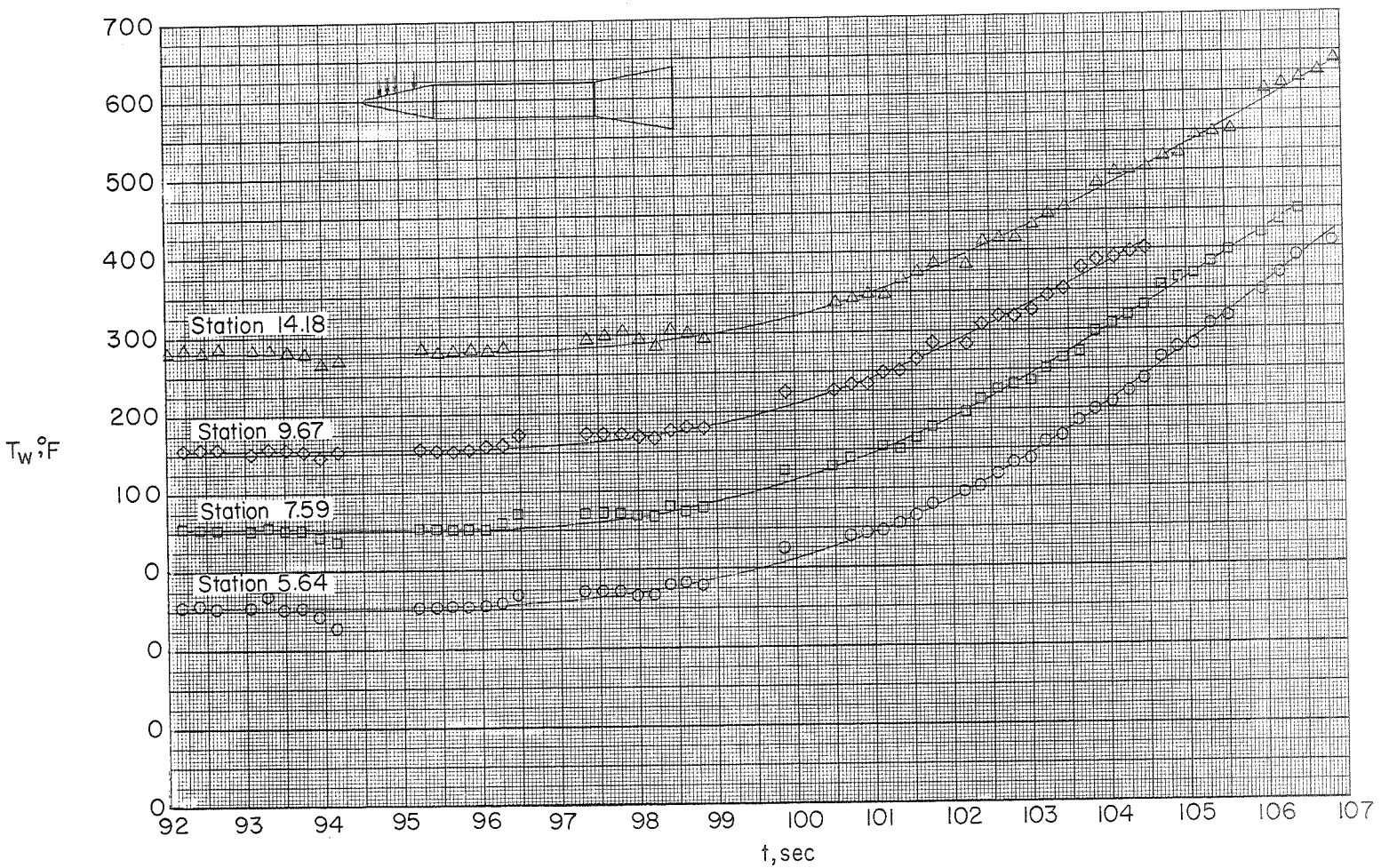

(a) Nose cone stations along upper thermocouple line.

Figure 13.- Time histories of skin temperatures over the period including the third- and fourth-stage burning.

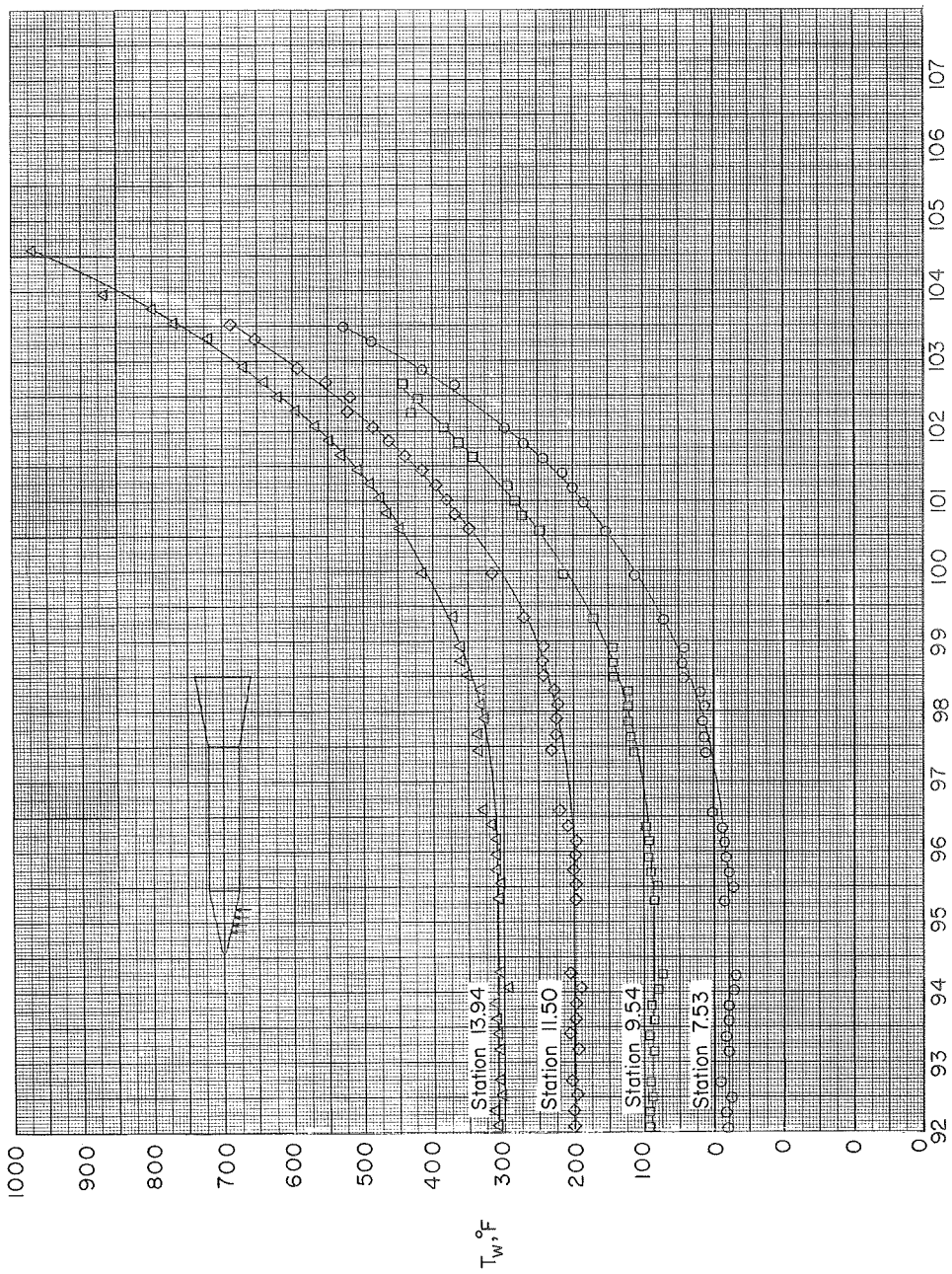

(b) Nose cone stations along lower thermocouple line.

Figure 13.- Continued.

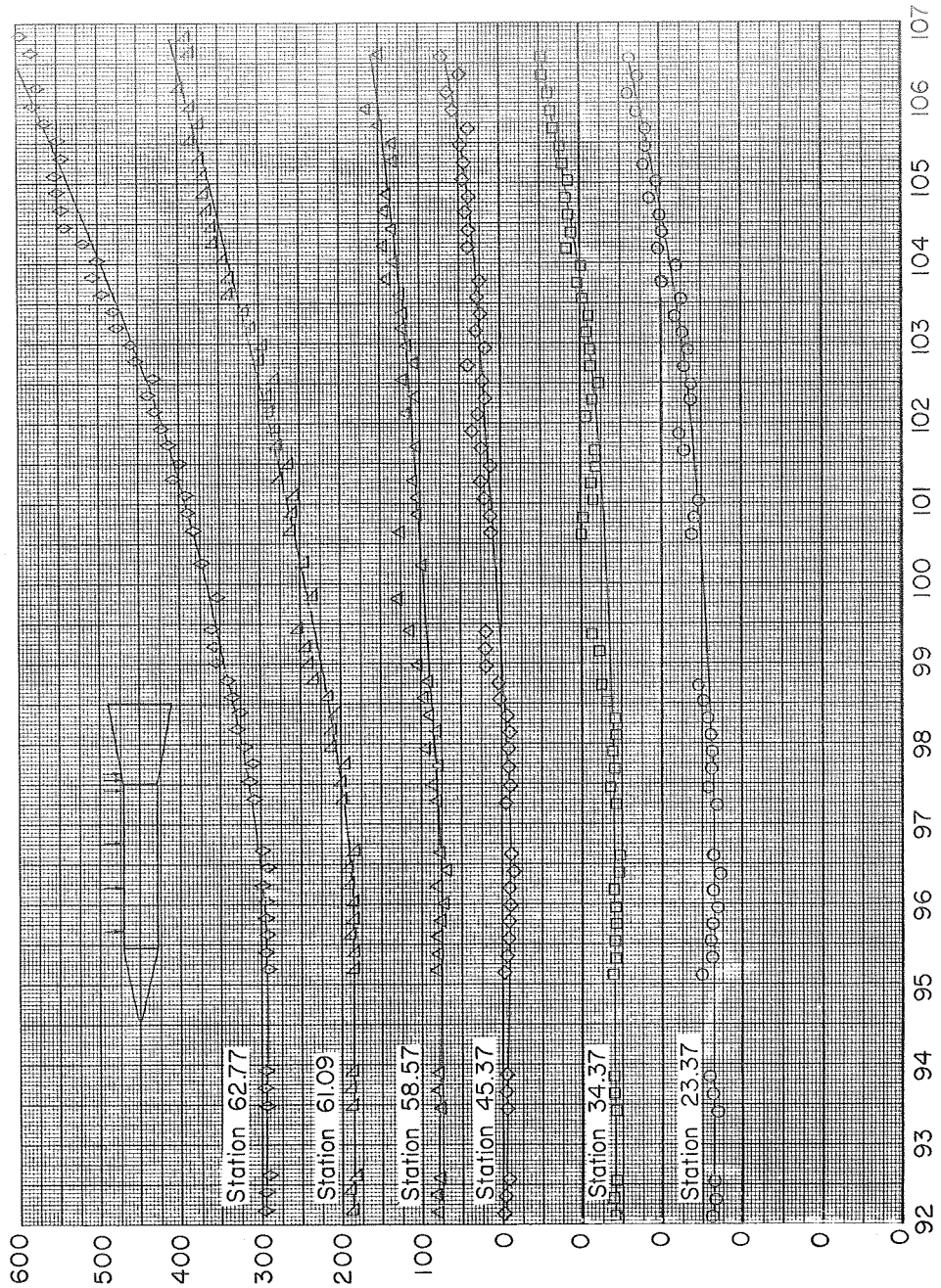

(c) Cylinder and forward flare stations.

Figure 13.- Continued.

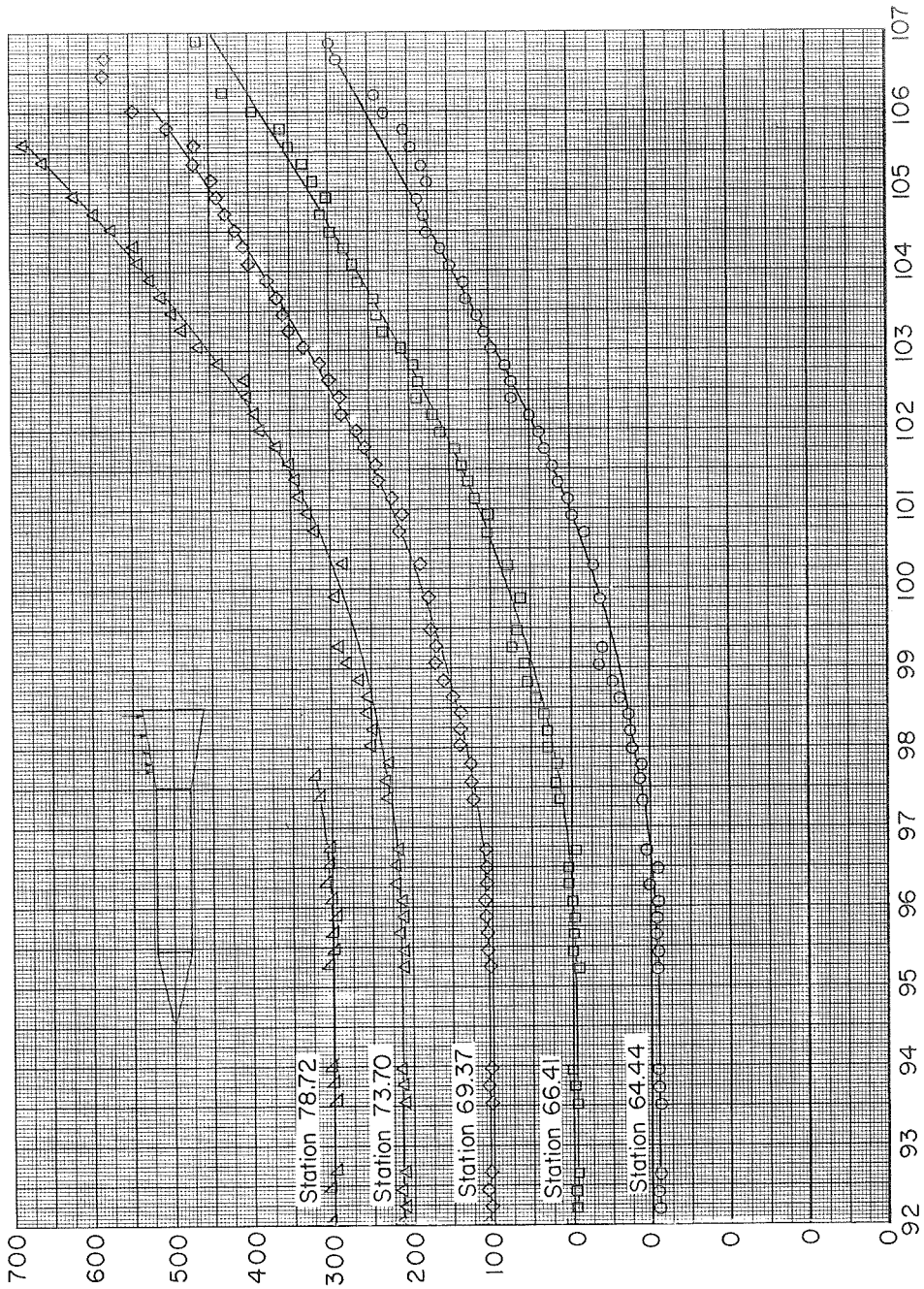

(d) Rearward flare stations.

Figure 13.- Concluded.

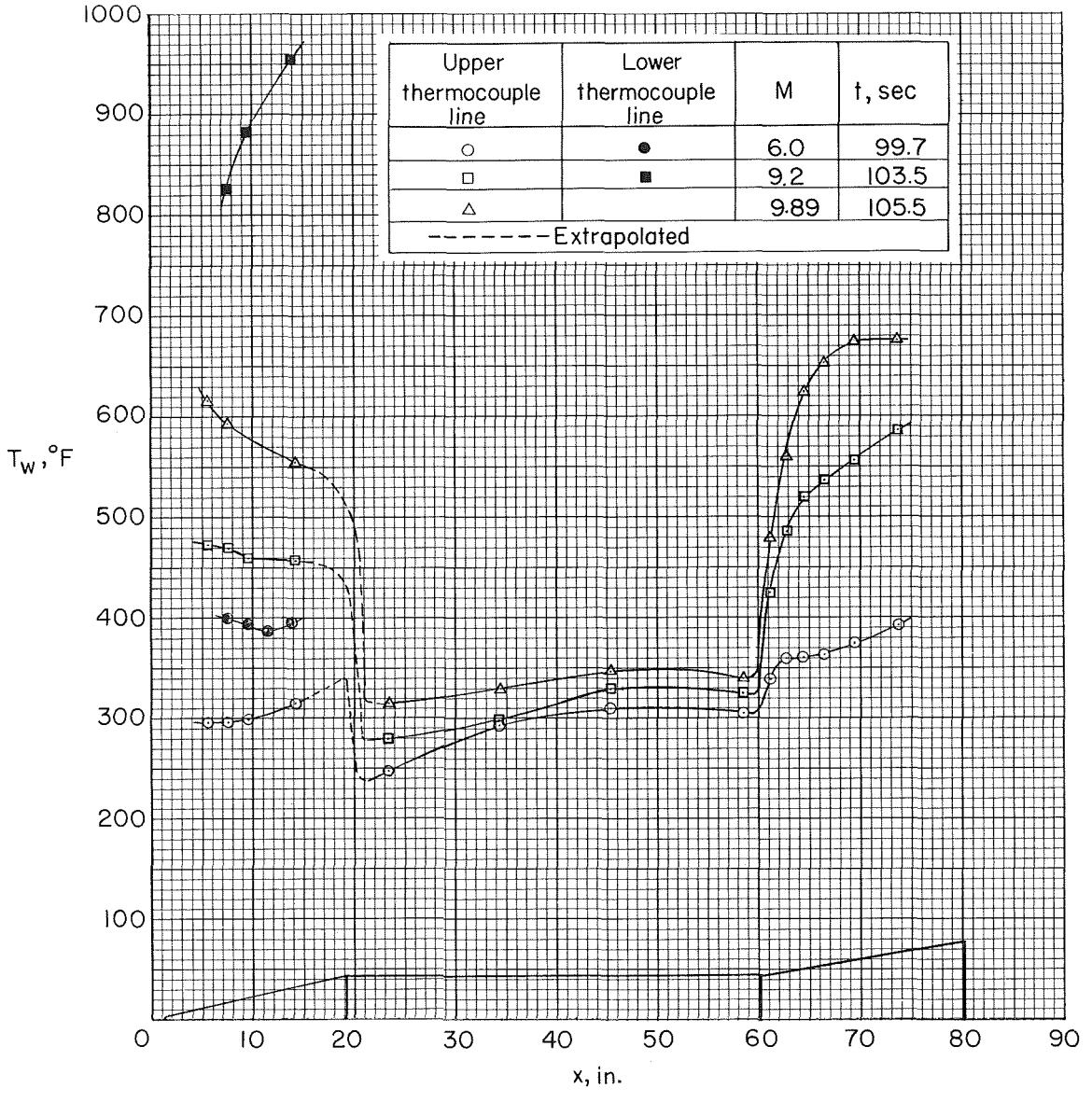

Figure 14.- Temperature distribution during high-speed portion of flight.

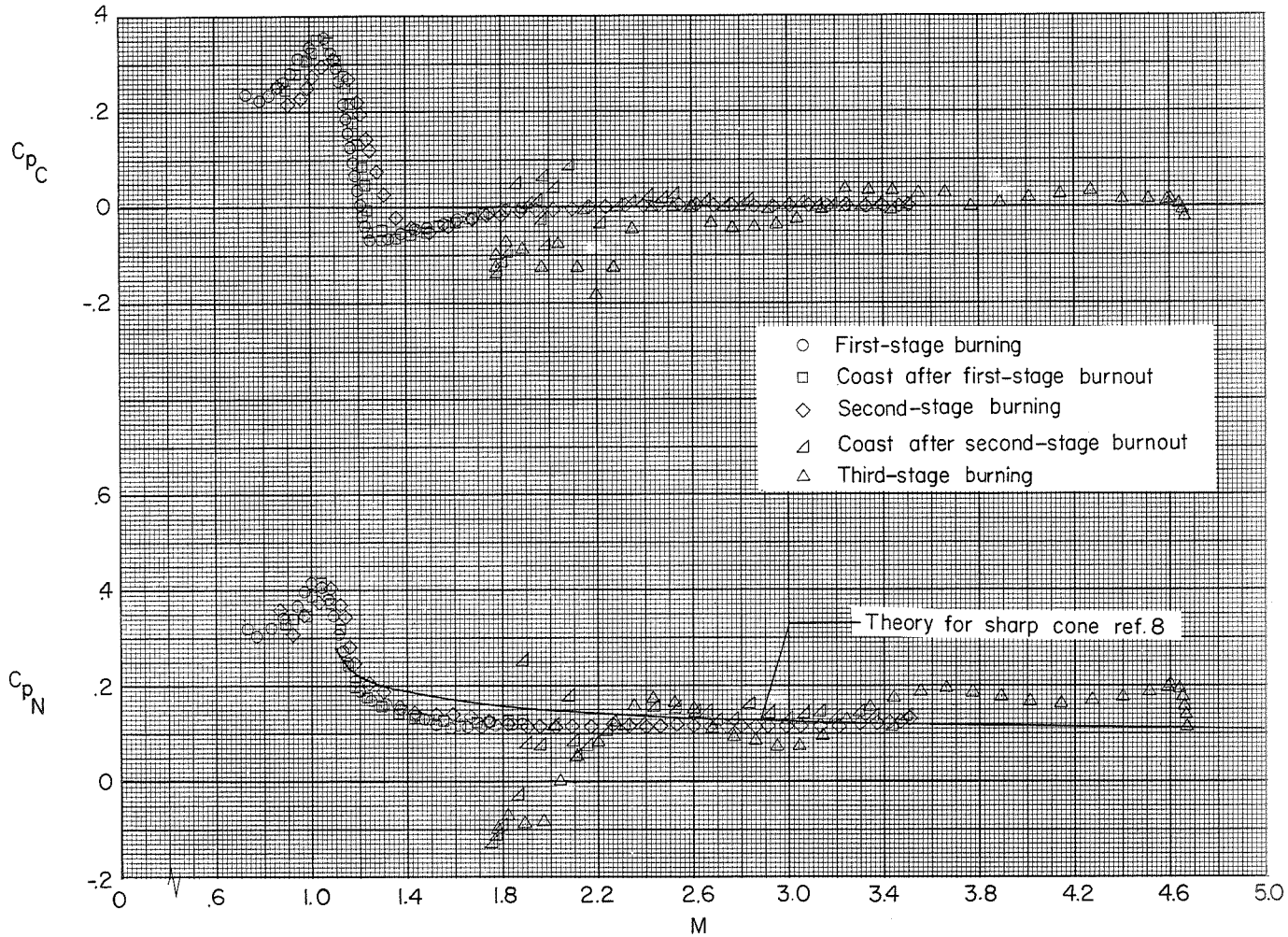

(a) Nose and cylinder stations.

Figure 15.- Pressure coefficients as a function of Mach number for the lower speed portion of flight.

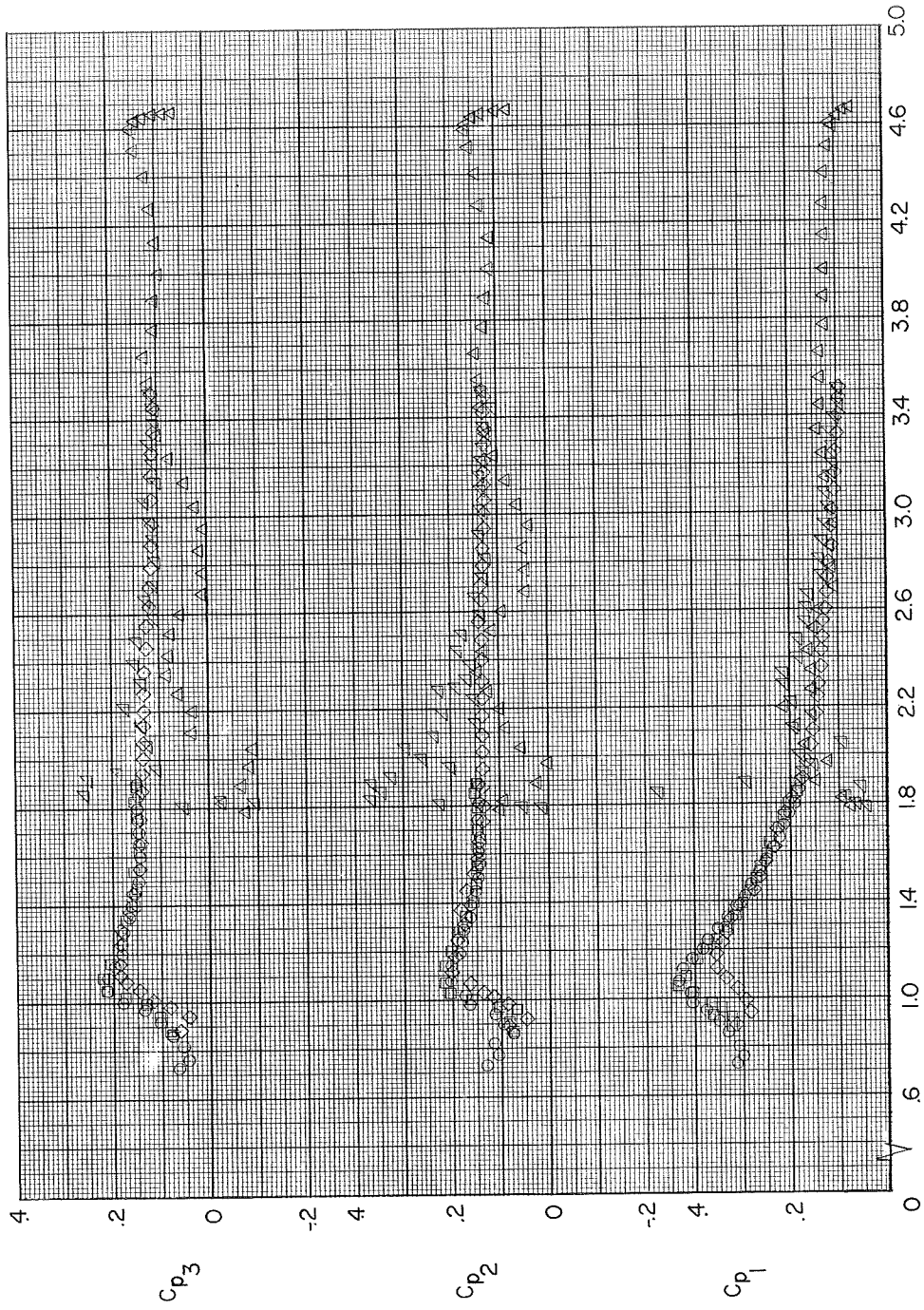

(b) Flare stations.

Figure 15.- Concluded.

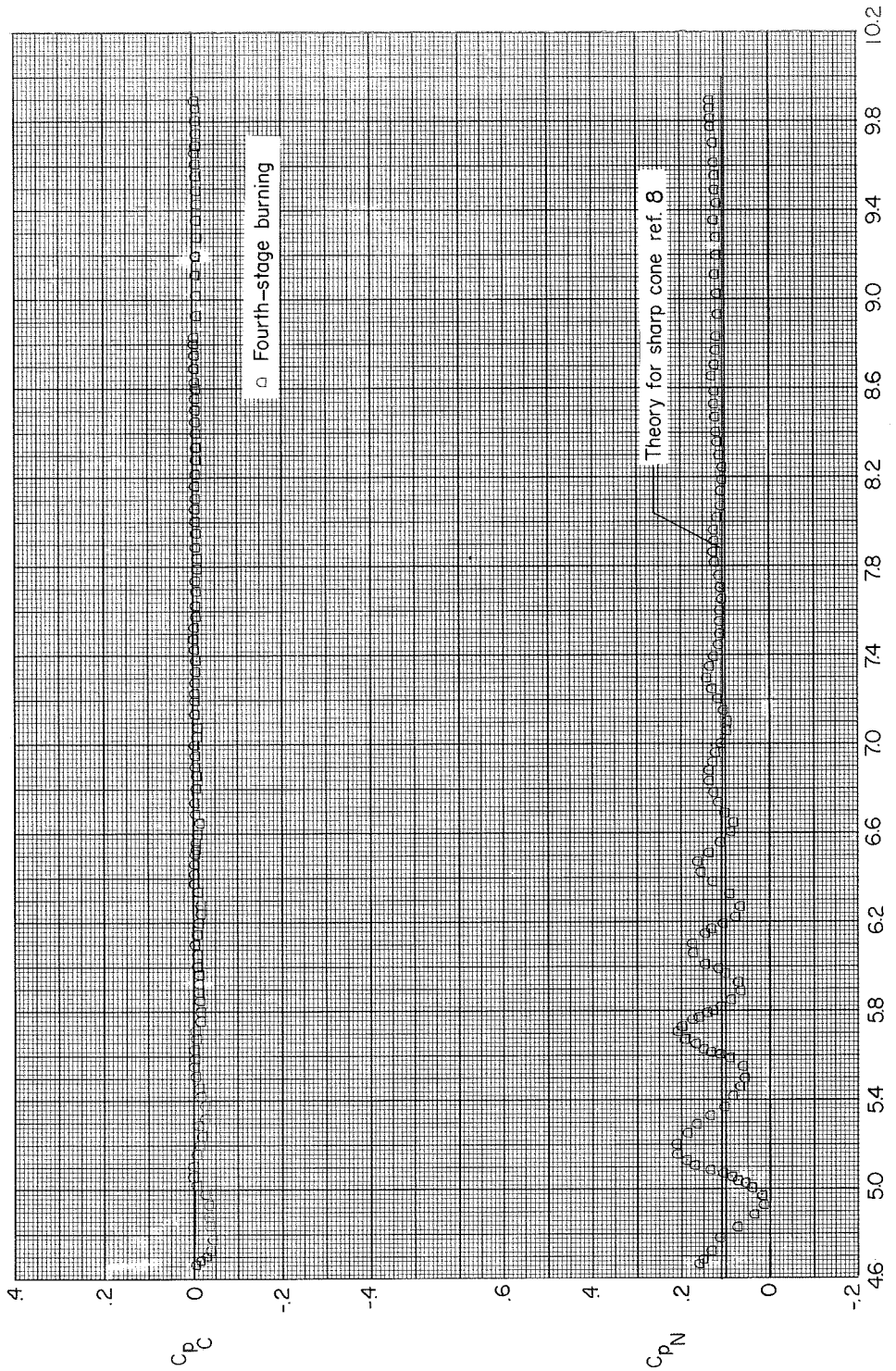

(a) Nose and cylinder stations.

Figure 16.- Pressure coefficients as a function of Mach number for the higher speed portion of flight.

(b) Flare stations.

Figure 16.- Concluded.

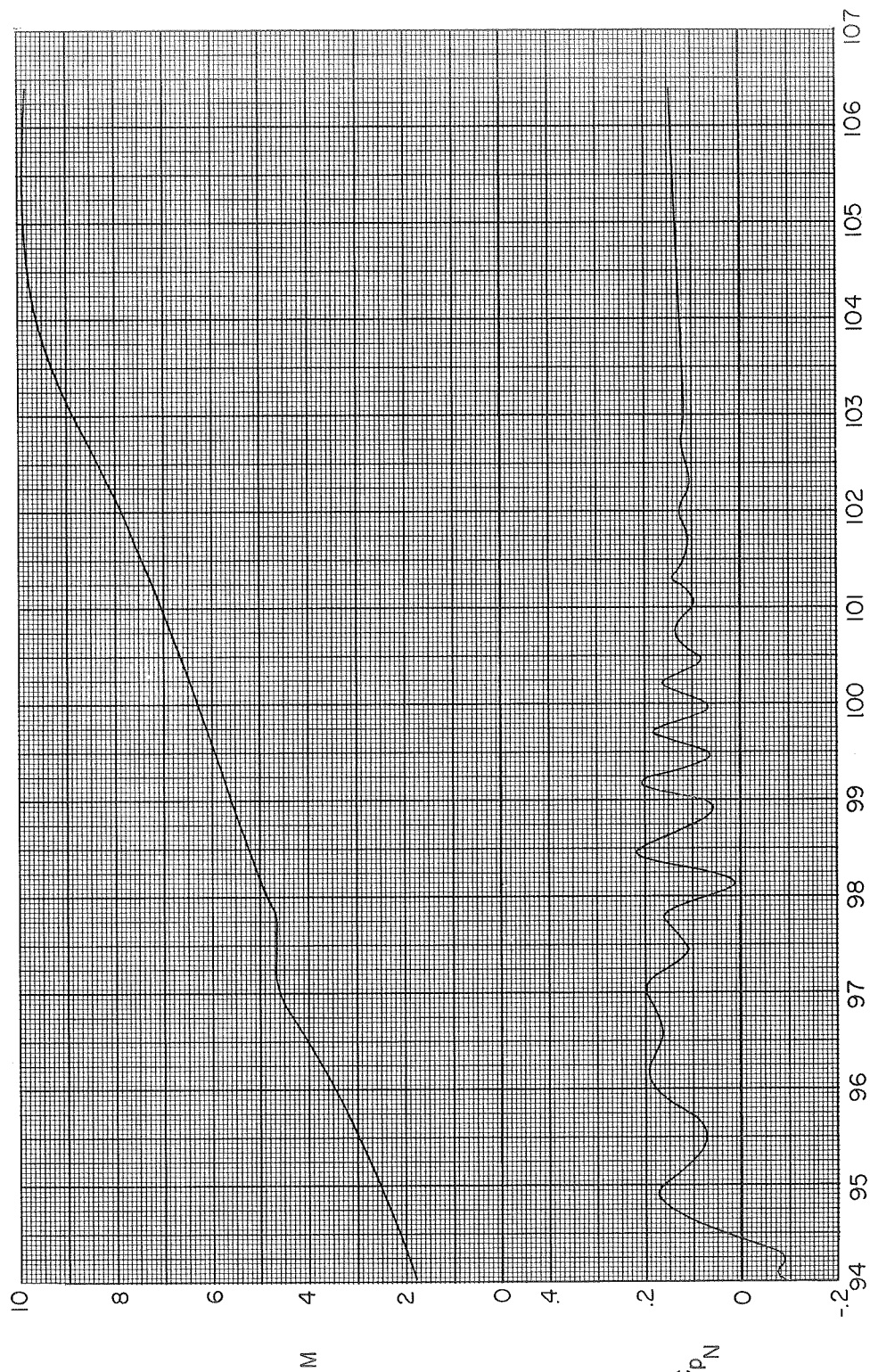

Figure 17.- Variation of nose pressure coefficient and Mach number with time during the high-speed portion of flight.